Construction of a T cell receptor signaling range for spontaneous development of autoimmune disease

Construction of a T-cell receptor signaling range for spontaneous development of autoimmune disease

Atsushi Tanaka[1,2,3,10], Shinji Maeda[1,4,10], Takashi Nomura[1,11], Mara Anais Llamas-Covarrubias[5,6], Satoshi Tanaka[1], Lin Jin[5], Ee Lyn Lim[2], Hiromasa Morikawa[2], Yohko Kitagawa[2], Shuji Akizuki[1], Yoshinaga Ito[1], Chihiro Fujimori[1], Keiji Hirota[1,2], Tosei Murase[1,2], Motomu Hashimoto[1], Junichi Higo[7], Rose Zamoyska[8], Ryuzo Ueda[9], Daron M. Standley[5], Noriko Sakaguchi[1,2], and Shimon Sakaguchi[1,2*]

[1]Department of Experimental Pathology, Institute for Frontier Medical Sciences, Kyoto University, Kyoto 606-8507, Japan.
[2]Laboratory of Experimental Immunology, WPI Immunology Frontier Research Center, Osaka University, Suita 565-0871, Japan
[3]Department of Frontier Research in Tumor Immunology, Center of Medical Innovation and Translational Research, Graduate School of Medicine, Osaka University, Osaka 565-0871, Japan
[4]Department of Respiratory Medicine, Allergy and Clinical Immunology, Nagoya City University Graduate School of Medical Sciences, Nagoya 467-8601, Japan
[5]Laboratory of Systems Immunology, WPI Immunology Frontier Research Center, Osaka University, Suita 565-0871, Japan
[6]Institute of Research in Biomedical Sciences, University Center of Health Sciences (CUCS), University of Guadalajara, Guadalajara 44340, Mexico
[7]Institute for Protein Research, Osaka University, Suita 565-0871, Japan
[8]Institute for Immunology and Infection Research, The University of Edinburgh, Edinburgh EH9 3JT, UK
[9]Department of Tumor Immunology, Aichi Medical University School of Medicine, Aichi 480-1195, Japan.
[10]These authors contributed equally to this work
[11]Current address: Department of Dermatology, Kyoto University Graduate School of Medicine, Kyoto 606-8507, Japan
*Correspondence: shimon@ifrec.osaka-u.ac.jp
Running title: Autoimmune range of TCR signaling

Abstract

Thymic selection and peripheral activation of conventional T (Tconv) and regulatory T (Treg) cells depend on TCR signaling, whose anomalies are causative of autoimmunity. Here, we expressed in normal mice mutated ZAP-70 molecules with different affinities for the CD3 chains, or wild-type ZAP-70 at graded expression levels under tetracycline-inducible control. Both manipulations reduced TCR signaling intensity to various extents and thereby rendered those normally deleted self-reactive thymocytes to become positively selected and form a highly autoimmune TCR repertoire. The signal reduction more profoundly affected Treg development and function because their TCR signaling was further attenuated by Foxp3 that physiologically repressed the expression of TCR-proximal signaling molecules, including ZAP-70, upon TCR stimulation. Consequently, the TCR signaling intensity reduced to a critical range generated pathogenic autoimmune Tconv cells and concurrently impaired Treg development/function, leading to spontaneous occurrence of autoimmune/inflammatory diseases, such as autoimmune arthritis and inflammatory bowel disease. These results provide a general model of how altered TCR signaling evokes autoimmune disease.

INTRODUCTION

T cells mediate a variety of common autoimmune diseases such as rheumatoid arthritis (RA) and type I diabetes. Both the production of autoreactive Tconv cells through T cell selection in the thymus and their pathogenic activation in the periphery critically depend on T-cell receptor (TCR) signaling upon recognition of self-peptide-bound major histocompatibility complexes (self-pMHCs). In addition, depending on the strength of the interaction between TCRs and self-pMHCs, some developing T cells differentiate into Treg cells, which specifically express the transcription factor Foxp3 and suppress the activation of pathogenic self-reactive T cells that have escaped thymic negative selection (Sakaguchi et al., 2020; Klein et al., 2019). It remains to be determined, however, how qualitative or quantitative alteration of TCR signaling itself should affect thymic generation of Treg and autoreactive Tconv cells and their peripheral functions to cause autoimmune diseases.

There is accumulating evidence in humans and rodents that genetic anomalies or variations in TCR-proximal signaling molecules, such as ZAP-70 and LAT, and also in the molecules interacting with them, such as PTPN22 and CBL family proteins, are causative of and predisposing to a variety of autoimmune diseases (Elder et al., 1994; Negishi et al., 1995; Aguado et al., 2002; Sommers et al., 2002; Sakaguchi et al., 2003; Siggs et al., 2007; Hsu et al., 2009; Bottini & Peterson, 2014; Chan et al., 2016; Keller et al., 2016; Au-Yeung et al., 2018). Among them, ZAP-70 mutations are unique in that they produce a wide spectrum of immunological disorders encompassing immunodeficiency, autoimmunity, immunopathology, and allergy in humans and rodents, by strictly affecting the T cell compartment (Elder et al., 1994; Negishi et al., 1995; Sakaguchi et al., 2003; Siggs et al., 2007; Hsu et al., 2009; Chan et al., 2016; Au-Yeung et al., 2018). Modulation of the structure of ZAP-70 or the amount of its expression can therefore be instrumental in deciphering how quantitative or qualitative alteration of TCR signaling impacts on thymic production and peripheral activation of self-reactive Tconv as well as Treg cells, consequently the balance between the two populations, to cause a plethora of autoimmune/inflammatory diseases.

Here we address the above issue by preparing mice expressing mutated ZAP-70 molecules with various binding affinities for the CD3 chains, or by expressing wild-type (WT) ZAP-70 molecules in ZAP-70-deficient mice at graded expression levels under tetracycline-inducible transcriptional control. Both manipulations indeed produced a similar spectrum of autoimmune/inflammatory diseases including autoimmune arthritis and inflammatory bowel disease (IBD), which immunologically resembled the human counterparts. The diseases spontaneously developed only when the TCR signaling intensity was reduced to a critical range in both systems. The results provide a general model of how attenuation of TCR signaling intensity via ZAP-70 and other TCR-proximal signaling molecules, whether due to genetically-induced structural anomalies or reduced expression of structurally intact forms, can be causative of autoimmune and other immunological disorders by affecting thymic development and peripheral function of Tconv and Treg cells.

RESULTS

ZAP-70 mutants with structural alterations reducing their affinity for CD3ζ chain

ZAP-70 has two tandemly arranged SH2 domains (N-terminal SH2 [N-SH2] and C-terminal SH2 [C-SH2] domains), which bind to doubly-phosphorylated ITAMs (pITAMs) of the CD3ζ and other CD3 chains. To assess the effects of ZAP-70 mutations on ZAP-70:CD3ζ-pITAM binding, we generated ZAP-70 SH2 domains with various mutations and measured their binding affinity for CD3ζ-pITAM (**Fig. 1A**). The arthritis-inducing SKG mutation (Sakaguchi et al., 2003), i.e., conversion of tryptophan 163 to cysteine (W163C), reduced the binding affinity of the SH2 domain by ~15-fold compared to WT SH2. H165A and W163A mutations showed ~8-fold and ~260-fold reductions, respectively. Further, alanine replacement mutations of aromatic residues, such as Y164 and F187, which were predicted to localize closely to W163 in 3D structure (**Fig. 1A**), showed more than 200-fold reduction, suggesting that these bulky aromatic residues were required for stabilizing the tandem SH2 domains in CD3ζ-pITAM binding.

Since the W163C, W163A, and H165A mutations are located near the border between the C-SH2 domain and the inter-SH2 linker (**Fig. 1A**), we performed the molecular dynamics (MD) simulation to analyze the stability of the tandem SH2 domains (**Fig. 1B**). The SH2 domains with or without mutations showed similar changes and stabilities when examined without a CD3ζ chain (**Fig. S1A**). In contrast, in the presence of CD3ζ-pITAM, SKG SH2 showed substantially greater distance (D_C) than WT SH2 between the amino acids forming the C-terminal phosphotyrosine binding (PTB) site (Hatada et al., 1995) and the phosphotyrosine pY4 of the CD3ζ-pITAM, while the distance (D_I) between the inter-SH2 PTB site and pY15 of the CD3ζ-pITAM showed no increase (**Fig. 1A-C, S1B, Video S1-2**). The SKG mutation produced no obvious spatial alteration of the kinase domain or the regions involved in autoinhibitory regulation (Au-Yeung et al., 2018) of ZAP-70, suggesting that the SKG mutation mainly affected the binding of the ZAP-70 C-terminal PTB pocket to CD3ζ-pITAM. Further, MD simulation of H165A SH2 with CD3ζ-pITAM revealed increases in D_C, whereas W163A SH2 showed substantial increases in both D_C and D_I with complete dissociation of the latter from CD3ζ-pITAM because of the absence of hydrogen bonds between CD3ζ-pITAM and PTB residues (**Fig. 1B, C, S1B, C, Video S1-4**).

Thus, the degree of change in the binding affinity of mutated ZAP-70 to CD3ζ closely correlated with their predicted extent of structural changes affecting the binding sites.

Spontaneous development of severe arthritis and colitis in ZAP-70 mutant mice

We next generated ZAP-70 knock-in mice (on the BALB/c background) (**Fig. S1D**) harboring the H165A or W163A mutation with higher or lower CD3ζ affinity, respectively, than SKG W163C mutation and compared them with BALB/c-background SKG mice in their potential to develop autoimmune disease. The amount of ZAP-70 protein in ZAC, SKG, and W163A $CD4^+$ Tconv cells was equivalently low (5.3, 4.5, and 5.4-fold, respectively, lower than in WT Tconv cells) (**Fig. S1E)**, possibly due to increased degradation of the mutant proteins (Tanaka et al., 2010).

SKG mice spontaneously developed autoimmune arthritis in microbially conventional environments but not under SPF conditions (Sakaguchi et al., 2003; Tanaka et al., 2010; Yoshitomi et al., 2005; Hashimoto et al., 2010). In contrast, the majority (~100%) of H165A mutant mice spontaneously succumbed to severe chronic autoimmune arthritis with overt joint swelling by 9 weeks of age even under an SPF condition (**Fig. 2A-C**). The arthritis typically started to develop at interphalangeal joints of the forepaws and progressed to wrists and ankles (**Fig. 2A, C**), with microscopically evident inflammatory proliferation of synoviocytes (synovitis) and pannus formation accompanying abundant cellular infiltration (**Fig. 2B**). H165A mutant mice also developed at a high (~60%) incidence macroscopically and microscopically evident colitis with severe diarrhea and systemic wasting (**Fig. 2D-F**). Based on these characteristic phenotypes, they are hereafter called ZAP-70 Arthritogenic and Colitogenic (ZAC) mice. W163A mutant mice, on the other hand, failed to develop clinically or histologically evident autoimmunity (**Fig. 2C, F**). Serologically, serum IgG1, IgG2a, and IgE concentrations and the titers of anti-cyclic citrullinated peptide (CCP), IgM rheumatoid factor (RF), and anti-gastric parietal cell autoantibodies were elevated in these ZAP-70 mutant mice to varying extents (**Fig. 2G**). Adoptive transfer of $CD4^+$ or $CD8^+$ T cells from WT, SKG, ZAC, or W163A mice into $RAG^{-/-}$ mice revealed that only $CD4^+$ T cells from ZAC or SKG mice were able to produce arthritis in the recipients (**Fig. 2H, S1F**). Moreover, mannan injection triggered arthritis in SKG mice as reported (Yoshitomi et al., 2005; Hashimoto et al., 2010), and increased arthritis severity in ZAC mice, but failed to elicit the disease in W163A mice (**Fig. 2I**).

Thus, 8~15-fold reduction of ZAP-70 affinity for CD3ζ by ZAC and SKG mutations resulted in the production of $CD4^+$ T cells with arthritogenic and/or colitogenic capacity, whereas ~260-fold reduction by W163A mutation did not. The degree of this affinity reduction also determined whether arthritis would develop spontaneously or require stimulation of innate immunity for triggering the disease. In addition, not only affinity reduction but also lower levels of ZAP-70 protein in the mutant mice may contribute to the disease induction.

Development of arthritogenic Th17 cells and impaired suppressive function of Treg cells in ZAC mice

All three ZAP-70 mutant strains showed significant reductions of $CD4^+$ and $CD8^+$ splenic T cells, with total splenocyte numbers comparable with those of WT mice (**Fig. 3A-B, S2A**). The percentages of $Foxp3^+$ Treg cells substantially increased in ZAC and SKG mice presumably as a secondary effect of their suffering from systemic inflammation. It contrasted with no Treg cell increase in non-autoimmune W163A mice with comparable levels of Foxp3 expression. Splenic Tconv and Treg cells in ZAC mice indeed highly expressed activation and proliferation markers (such as CD44 and Ki67) (**Fig. 3B, S2B-C**) as previously shown for SKG mice (Hirota et al., 2007).

ZAC $CD4^+$ Tconv cells actively produced IFNγ, IL-17A, and IL-4, and highly expressed CXCR3 and CCR6, reflecting their particular Th differentiated states (**Fig. 3C-D, S2B, D**). In Peyer's patches, ZAC mice showed a notable increase of $CXCR5^{hi}PD\text{-}1^{hi}$ T follicular helper (Tfh) cells highly expressing IL-4 (**Fig. 3D-E**). ZAC mice deficient in IL-17A did not develop arthritis or colitis, albeit some mice slowly developed mild arthritis after 14 weeks of age (**Fig. 3F**). Notably, IL-$17A^{-/-}$ ZAC $CD4^+$ T cells showed an increased production of IL-17F (**Fig. S2D**), suggesting that IL-17F might partially compensate for the loss of IL-17A in the late-onset arthritis in IL-$17A^{-/-}$ ZAC mice.

Treg cells in ZAC mice were impaired in *in vitro* suppressive function (**Fig. 3G**), despite their normal or high expressions of Treg-function-associated molecules (**Fig. S2C**), as were W163A (**Fig. S2E**) or SKG Treg cells (Tanaka et al., 2010). *In vivo*, cell transfer of WT Treg cells into ZAC mice before disease onset prevented both arthritis and colitis in a dose-dependent fashion (**Fig. 3H**). The transferred WT Treg cells persisted dominantly over endogenous Treg cells in the recipient ZAC mice (**Fig. 3I, S2F**). Further,

co-transfer of a small number ($2x10^5$) of WT Treg cells along with $1x10^6$ ZAC $CD4^+$ T cells prevented arthritis, colitis, and splenomegaly in $RAG^{-/-}$ recipient mice (**Fig. 3J, S2G-H**).

Thus, despite the fact that autoimmune ZAC Tconv cells are sensitive to suppression by normal Treg cells, dysfunctional ZAC Treg cells allow them to become activated and differentiate into Th17 and other effector T cells to elicit arthritis and colitis.

Single cell analysis of the transcriptome and the TCR clonotype of Tconv and Treg cells in ZAC mice

To further characterize ZAC Tconv and Treg cells by gene expression, we performed single-cell RNA sequencing (scRNA-seq) of transcriptomes and TCR clonotypes on splenic Tconv and Treg cells in WT and ZAC mice. After quality control and batch correction of the samples, $CD3^+$ cells were segregated into 10 clusters based on gene expression similarities (**Fig. 4A, S3A**). Clusters 0 and 4-7 were mostly composed of Tconv cells while Clusters 1-3 and 8-9 were of Treg cells expressing Foxp3 and other Treg signature genes, e.g., *Il2ra* and *Ikzf2* (**Fig. 4B-D, S3B**). Differentially expressed genes and Th signature genes in each cluster showed that Cluster 6 and 7 were mostly composed of ZAC Tconv cells, with unique expression of *Il17* and *Rorc* along with other Th17 associated genes such as *Ccr6* in Cluster 6 and predominant expression of Th1 and Th2 related genes such as *Il4*, *Ifng*, and *Tbx21* in Cluster 7 (**Fig. 4C-D, S3B**). Pseudotime analysis of Tconv cells based on gene expression changes enabled an inference of a trajectory of naïve cells (Clusters 0 and 5) differentiating into Cluster 6 and 7 (**Fig. S3C**).

Single cell TCR clonotyping of splenic Tconv and Treg cells revealed that effector Tconv, naïve Treg, and effector Treg populations in ZAC mice were less diverse than the counterparts in WT mice as indicated by low inverse Simpson indexes (**Fig. 5A**). The frequencies of individual dominant TCR clones in Tconv and Treg cells were much higher in ZAC mice, indicating their clonotypic expansion (**Fig. 5B, Table S1**). Among the annotated clusters in Fig. 4A, Cluster 6, which was mostly composed of ZAC Tconv cells, had the lowest TCR repertoire diversity (**Fig. 5C**). In addition, the top 10 highly frequent clonotypes of ZAC Tconv cells in the spleen overlapped broadly with the top 10 clonotypes in Cluster 6 (spleen), Tconv cells in the draining popliteal lymph nodes, and those in inflamed joints in individual mice, as also the case with the 10 top clonotypes of

ZAC Treg cells (**Fig. 5D-E, S3D-E, Table S1**). In addition, ZAC Treg and Tconv cells shared an increased ratio of common TCR clonotypes, which were mostly found in Cluster 6 (**Fig. 5F-G, Table S1**). Notably, ZAC Treg cells highly expressed Helios and Nrp1, potential markers for thymic Treg cells (**Fig. S2C**); however, Helios$^-$Foxp3$^-$ Tconv cells in ZAC mice were able to become Helios$^+$Foxp3$^+$ Treg cells upon transfer into RAG$^{-/-}$ mice (**Fig. S3F**). This suggested that some of self-reactive Tconv cells could differentiate into Helios$^+$ Treg cells in the periphery of ZAC mice.

Thus, Tconv cells in ZAC mice clonally expanded, differentiated into Th17 cells, and mediated arthritis. ZAC Treg cells also showed similar clonotypic expansion.

Altered thymic selection of Tconv and Treg cells in ZAP-70 mutant mice

In all three ZAP-70 mutant strains, the numbers of CD4$^+$CD8$^-$ (CD4 single-positive [CD4SP]) and CD4$^-$CD8$^+$ (CD8SP) thymocytes were reduced significantly, with total thymocyte numbers comparable between mutant and WT mice (**Fig. 6A-B, S4A**). Among CD4SP thymocytes, Foxp3$^+$Treg cells were severely diminished in the mutant strains (**Fig. 6A-B, S4A**). CD4SP and Foxp3$^+$Treg cells in SKG mice showed slightly better efficiency in their selection or survival compared to other mutant strains. CD4$^+$CD8$^+$ (double-positive [DP]) and CD4SP thymocytes from ZAP-70 mutant mice were low in the expression of TCRβ as well as CD69 (**Fig. S4B**), which are upregulated following TCR ligation (Anderson et al., 1999), and also in CD5 as reported in SKG mice (Ashouri et al., 2019). Further, compared with WT mice, DP thymocytes in ZAC, SKG, and W163A strains were resistant to TCR stimulation-induced down-modulation of TCR (Schrum et al., 2003) (**Fig. 6C**), in accord with the attenuated TCR signaling in these strains. Assessment of the ratios of TCRβ$^+$CD4SP thymocytes expressing TCR Vβ subfamilies reactive with endogenous MMTV superantigens, hence normally deleted in WT BALB/c mice (Herman et al., 1991), revealed that they were significantly increased in the thymus and periphery in all three ZAP-70 mutant strains (**Fig. 6D**, **Fig. S4C**). Although the number of thymic Treg cells in ZAC mice was too small to analyze, their peripheral Treg cells showed a profound increase in the ratio of such normally deleted T cells (**Fig. S4D**). Furthermore, in chicken ovalbumin (OVA)-specific DO11.10 TCR transgenic RAG2$^{-/-}$ mice (Kawahata et al., 2002), systemic transgenic expression of OVA negatively selected CD4SP thymocytes on the WT background whereas it positively

selected CD4SP thymocytes on the ZAC background (**Fig. 6E-F**). In contrast, thymic Treg cells, which were absent in DO11.10 $RAG^{-/-}$ mice, were positively selected by the OVA expression on the WT background, but not on the ZAC background.

Functionally, peripheral Tconv cells from ZAC and other ZAP-70 mutant mice were impaired in phosphorylation of ERK at a down-stream of TCR signaling (**Fig. S4E**) and much less proliferative than WT Tconv cells upon *in vitro* anti-CD3 stimulation (**Fig. 6G**). However, when the cells were cultured simply on autologous antigen-presenting cells (i.e., autologous mixed lymphocyte culture), ZAC and SKG Tconv cells exhibited more active proliferation than WT or W163A $CD4^+$ Tconv cells (**Fig. 6H**). Similar results were obtained with whole $CD4^+$ T cells including Treg cells from these mice indicating that Treg cells failed to suppress the proliferation of respective Tconv populations (**Fig. S4F-G**). Moreover, transfer of whole $CD4^+$ T cells into syngeneic $RAG^{-/-}$ mice revealed more active homeostatic proliferation of ZAC and SKG $CD4^+$ T cells compared with WT or W163A $CD4^+$ T cells (**Fig. 6I**).

Taken together, signal reduction through mutated ZAP-70 hampered thymic positive selection of developing Tconv cells, producing T-lymphopenia, and also hindered negative selection of those normally deleted Tconv cells. The reduction similarly and more profoundly affected positive/negative selection of Tregs cells, severely reducing thymic Treg cell production. The aberrantly selected Tconv cells included those highly responding to self-antigens *in vivo* and *in vitro* despite their impaired TCR signaling.

Foxp3-dependent Treg-specific physiological down-regulation of ZAP-70 and other signaling molecules expression

We next examined possible differences in the mode of TCR signaling between Treg and Tconv cells in WT and ZAC mice. Notably, WT Tconv cells up-regulated ZAP-70 upon *in vitro* TCR stimulation whereas WT Treg cells down-regulated the expression, but expressed Nur77, an immediate early gene upon TCR stimulation, to a similar extent (**Fig. 7A**). In contrast, ZAC Tconv and Treg cells hardly up- or down-regulated ZAP-70 expression upon TCR stimulation, which upregulated Nur77 close to the WT level in ZAC Tconv cells but not in ZAC Treg cells.

In WT Treg cells, Foxp3 bound to the promoter region of *ZAP-70* and repressed *ZAP-70* transcription upon TCR stimulation (Ohkura et al., 2012; Tanaka et al., 2020).

Foxp3 bound to the promoter regions of other genes encoding TCR-proximal and -distal signaling molecules, two thirds of which showed slightly lower basal expression levels in Treg cells compared with Tconv cells (**Fig. 7B-C**). For example, Treg cells were physiologically lower in the expression levels of Lck protein and active Lck (pY394-Lck), the most proximal TCR signaling kinase, in both WT and ZAC mice (**Fig. S4H-I**). Similar to *Zap70*, other Foxp3-bound genes, such as *Cd45*, *Ptpn22*, *Slp76*, and *Cblb*, were down-regulated in Treg cells and up-regulated in Tconv cells upon TCR stimulation (**Fig. 7C**).

To assess functional roles of Treg-specific ZAP-70 down-regulation, we generated ZAP-70-inducible mice using the transgenes expressing tetracycline (Tet)-inducible human ZAP-70 (hZAP-70) with eGFP and reverse tetracycline transactivator (rtTA) under the control of human CD2 promoter (Legname et al., 2000) (designated $rtTA^+$ Tet-$hZAP\text{-}70^+$ mice) (**Fig. S5A**). *In vitro* incubation of $rtTA^+$ Tet-$hZAP\text{-}70^+$ Tconv cells with graded doses of doxycycline (Dox) showed a close correlation between hZAP-70 protein and GFP expression (**Fig. S5B-D**). Upon TCR stimulation, WT Treg cells were hypo-proliferative *in vitro* (Takahashi et al., 1998; Thornton & Shevach; 1998), whereas GFP^+ (i.e., hZAP-70 overexpressing) Treg cells proliferated as actively as $CD4^+$ Tconv cells (**Fig. 7D**), indicating a contribution of the Treg-intrinsic low ZAP-70 expression to the *in vitro* hypoproliferation of Treg cells.

Thus, Treg cells specifically down-regulate some of the key TCR signaling molecules mainly, if not solely, by Foxp3-dependent gene repression, thereby controlling their responsiveness to TCR stimulation. ZAP-70 mutations, when combined with this Treg-intrinsic TCR signaling regulation, more severely impair TCR signaling in Treg than in Tconv cells; it might also hamper the TCR-dependent activation of Foxp3 to control the expression of ZAP-70 and other signaling molecules in Treg cells.

Spontaneous development of autoimmune diseases in mice expressing a low amount of normal ZAP-70

The above results with ZAP-70 mutant mice posed a question whether a qualitative alteration due to a specific conformational change in the ZAP-70 molecule (and resulting altered interactions with other signaling molecules) or a mere reduction of the quantity of TCR signal through ZAP-70 was responsible for the autoimmune induction. To address the issue, we expressed graded amounts of structurally intact hZAP-70 in

rtTA$^+$ Tet-hZAP-70$^+$ mice on the BALB/c background with endogenous ZAP-70 deficiency (hereafter called Tet-on ZAP mice). By continuous feeding with Dox-containing food (Dox 0.5 [0.5mg/g of Dox in food] or Dox 2.0 [2.0 mg/g]) for 9 weeks, Dox 0.5 Tet-on ZAP mice (hereafter called Dox 0.5 mice) showed shorter survivals (~50% mortality during 2-month observation) than Dox 2.0 mice (**Fig. 8A**), with failure to gain weight (**Fig. 8B**), and spontaneously developed chronically progressing joint swelling at a high (~80%) cumulative incidence (**Fig. 8C-D**). The arthritis was histologically evident with synovitis and destruction of the cartilage and bone (**Fig. 8E-G**). The mice also developed other clinically and histologically evident autoimmune/inflammatory lesions (**Fig. 8E-G, S5E**), including dermatitis, interstitial pneumonitis, myositis, and colitis with severe diarrhea. It was also noted that they failed to develop autoimmune gastritis, which is the most frequent autoimmunity induced by Treg depletion on the BALB/c background (Sakaguchi et al., 1985), presumably because of TCR repertoire change due to the mutation (Tanaka et al., 2010). Serologically, Dox 0.5 mice developed higher concentrations of serum IgG than Dox 2.0 mice with similar increases in IgE, IgM RF, and anti-CCP antibody titers (**Fig. 8H**). Both Treg and Tconv cells were highly activated in Dox 0.5 mice (**Fig. 8I, S5F**), and developed larger numbers of Th17 and Th1 cells (**Fig. 8J**). Thus, reduced expression of structurally normal ZAP-70 molecules resulted in spontaneous development of a wide spectrum of autoimmune/inflammatory diseases, including arthritis and colitis, as observed in ZAC mice.

Graded expression of normal ZAP-70 alters thymic selection of Tconv and Treg cells

In the thymus, Dox 2.0 mice expressed higher levels of GFP and produced larger numbers of DP and mature (i.e., TCRβ-chain expressing) CD4SP and CD8SP thymocytes as well as Foxp3$^+$CD4SP thymocytes than Dox 0.5 mice (**Fig. 9A-C, S5G)**. In the periphery, the number of CD4$^+$ and CD8$^+$ splenic T cells were lower in Dox 0.5 than in BALB/c mice, but harbored a larger number of Foxp3$^+$ Treg cells presumably as a secondary effect of systemic inflammation (**Fig. 9C, S5H**). Notably, the percentages of TCRβ$^+$CD4SP and CD8SP thymocytes among whole thymocytes in these Dox-treated mice were directly proportional to the levels of GFP expression, hence ZAP-70 expression (**Fig. S5I**), in a wide range (e.g., in 0.03~3% range of CD4SP thymocytes produced) (**Fig. 9D**). Indeed, compared with Dox 0.5 mice, DP thymocytes in Dox 2.0 mice expressed

higher levels of TCRβ, and also CD5 and CD69 (**Fig. S5J**). Similarly, the development of Foxp3$^+$CD4SP thymocytes was directly proportional (in 1~30% range of CD4SP thymocytes produced) to the levels of GFP expression especially in Dox 2.0 mice, which developed ten times higher numbers of Foxp3$^+$CD4SP thymocytes than Dox 0.5 mice (**Fig. 9C-D, S5G**).

Assessment of thymic negative selection revealed that the ratios of CD4SP thymocytes expressing self-reactive TCR Vβ3, 5, and 11 subfamilies were inversely proportional to GFP levels in a wide range (e.g., 0.8~6% for Vβ3$^+$ cells among CD4SP thymocytes); i.e., the higher was the GFP expression, the more efficiently deleted were such Vβ-expressing cells, approaching their very low levels in normal BALB/c mice (**Fig. 9E**). In the periphery, Dox 0.5 mice compared with Dox 2.0 or WT mice indeed possessed significantly higher proportions of CD4$^+$ Tconv and Treg cells expressing such self-reactive Vβs (**Fig. 9F**).

Functionally, both Dox 0.5 and Dox 2.0 CD4$^+$ T cells were profoundly hyporesponsive to anti-CD3 stimulation *in vitro* (**Fig. 9G**). However, upon transfer of CD4$^+$ or CD8$^+$ T cells from Dox 0.5 or Dox 2.0 mice into RAG$^{-/-}$ mice that were continuously fed with Dox 0.5 food, Dox 0.5 donor-derived CD4$^+$ T cells expanded more vigorously than Dox 2.0 or normal BALB/c CD4$^+$ T cells, suggesting higher self-reactivity of the former than the latter (**Fig. 9H)**. In addition, *in vitro* suppressive activity of Dox 0.5 or 2.0 Treg cells was much less potent than BALB/c Treg cells even in the presence of a high Dox dose (**Fig. 9I**). These CD4$^+$ T cells in Dox 0.5 and Dox 2.0 mice, when compared with those in WT mice, showed ~15 and ~7-fold reductions, respectively, in ZAP-70 expression levels (**Fig. S5K**).

Thus, the efficiencies of both positive and negative selection of CD4SP and CD8SP thymocytes and Treg cells are closely dependent on the quantity of intact ZAP-70 expressed in developing T cells. The lower the ZAP-70 expression, the more are self-reactive Tconv and Treg cells positively selected and the less negatively selected. The reduction of ZAP-70 expression also impairs the function of Treg cells, allowing an expansion of self-reactive Tconv cells. It was also suggested that disease induction by quantitative reduction of WT ZAP-70 might require a much lower amount of WT ZAP-70 compared to mutant ZAP-70 molecules, which were reduced ~5-fold in mutant mice (see above).

Low ZAP-70 expression impairs Treg suppression and alters Tconv specificity for autoimmune disease induction

We next attempted to determine how the altered TCR repertoire of developing T cells and the impaired functions of both Treg and Tconv cells, as shown above, contributed to actual autoimmune disease development in Tet-on ZAP mice.

First, we transferred to $RAG^{-/-}$ mice the same number of CD4SP thymocyte suspensions from individual mice Dox 0.5- or 2.0-treated for 4 weeks, and fed the recipients with Dox 0.5 food for 3 months (**Fig. 10A**). Arthritis developed mostly in the recipients of thymocytes from Dox 0.5 mice, with disease incidence and severity showing an inverse correlation with the levels of GFP expression in donor CD4SP thymocytes at the time of transfer; i.e., GFP^{low}CD4SP thymocytes predominantly elicited arthritis in the recipients. Similarly, CD4SP thymocytes that induced histologically evident synovitis, interstitial pneumonitis and/or colitis in the recipients had significantly lower GFP expression than those which failed to produce these diseases (**Fig. 10B**).

To determine next whether the autoimmune-inducing repertoire and activity of thymocytes, as shown above, were retained in the periphery, we transferred into $RAG^{-/-}$ mice Treg-depleted $CD4^+CD25^-$ or non-depleted $CD4^+$ splenic T cell suspensions from the mice Dox-treated for 9 weeks as shown in Fig. 8, with continued Dox treatment of the recipient mice for 12 weeks. Transfer of $CD4^+CD25^-$ T cells from Dox 0.5 mice reduced the survival of the recipients while cell transfer from Dox 2.0 mice did not (**Fig. 10C**). The former induced autoimmune diseases at higher incidences and in more severe forms than the latter; further, the spectrum of autoimmune diseases in these cell transfers was different from the one induced by BALB/c $CD4^+CD25^-$ cell transfer, which induced autoimmune gastritis predominantly (Sakaguchi et al., 1995) (**Fig. 10D-E**). In addition, when the $RAG^{-/-}$ recipients of $CD4^+CD25^-$ T cells from arthritis-bearing Dox 0.5 mice were kept treated with the Dox dose 0.5 or 2.0, either treatment equivalently induced arthritis, whereas those from Dox 2.0 mice hardly developed the disease irrespective of the Dox doses for treating the recipients (**Fig. 10F**). As a control, when whole splenocytes from Dox-untreated Tet-on ZAP mice were transferred into $RAG^{-/-}$ recipients and fed with Dox 0.5 food, they failed to induce autoimmune arthritis (**Fig. 10F**).

Thus, Treg depletion revealed that the autoimmune-inducing TCR repertoire formed in the thymus, but not the efficacy of TCR-signaling dependent activation of peripheral Tconv cells, was essential for the autoimmunity in Tet-on ZAP mice.

The lower incidence and less severity of autoimmune disease in the recipients of $CD4^+$ Tconv cells compared with those of $CD4^+CD25^-$ Tconv cells in the above experiments indicated possible contribution of Treg cells. When the same number of $CD25^{high}CD4^+$ Treg cells from Dox 0.5 mice or normal BALB/c mice were transferred into Dox 0.5 mice, the former was indeed much less potent than the latter in suppressing arthritis development (**Fig. 10G**).

Taken together, thymic generation of Tconv cells with autoimmune TCR specificities as well as impaired Treg development and function are critically required to evoke and determine the disease spectrum and severity of autoimmunity caused by low ZAP-70 expression.

DISCUSSION

As the main findings in this study, a similar spectrum of autoimmune/inflammatory diseases spontaneously developed when TCR signaling intensity was reduced to a similar extent by changing the structure of ZAP-70 or the expression level of normal ZAP-70. Further, both manipulations altered the thymic formation of the TCR repertoire of self-reactive Tconv cells and concurrently hampered thymic generation and peripheral function of Treg cells, hence affecting the balance between the two populations, to evoke the diseases.

Tconv cells generated in the thymus at a low TCR signaling range acquired a highly self-reactive TCR repertoire as shown in both ZAP-70 mutants and Tet-on ZAP mice. In the latter model, for example, low-level ZAP-70 expression at a low Dox dose predominantly generated (i.e., positively selected) T cells reactive to endogenous super-antigens; negative selection of such self-reactive T cells gradually became more effective in proportion to the increase of ZAP-70 expression, nearing their low numbers in ZAP-70-intact mice. Tconv cells in ZAP-70-low Tet-on ZAP mice and ZAP-70 mutant mice were also functionally self-reactive as suggested by their high *in vitro* and *in vivo* proliferative activity against autologous APCs physiologically presenting endogenous self-antigens. Such self-reactive Tconv cells appeared to stimulate APCs to secrete IL-6 and other

cytokines, driving themselves to differentiate into Th17 and other effector T cells (Hirota et al., 2007). Low thymic output hence partially lymphopenic environment in ZAP-70-altered mice could also favor clonal expansion of such self-reactive Tconv cells (Liston et al., 2008). It is thus likely that in the ZAP-70-altered mice, some T cells expressing low-affinity TCRs for self-pMHCs are not positively selected because TCR signal intensity is reduced below the threshold required for positive selection. The signal reduction, on the other hand, enables T cells strongly reactive to self-pMHC, hence normally deleted, to survive (i.e., escape negative selection). The resulting shift of the whole TCR repertoire of Tconv cells towards higher affinities for thymic self-pMHCs, hence more self-reactive than ZAP-70-intact Tconv cells, changes the potential spectrum of T cell-dependent autoimmune and immunopathological diseases especially towards more systemic ones including autoimmune arthritis.

In mature Treg cells, the basal expression levels of some TCR signaling molecules, such as Lck, are kept low; upon TCR stimulation, Foxp3 further represses ZAP-70 and some other TCR-proximal signaling molecules by binding to their gene promoter regions (Ohkura et al., 2012; Morikawa et al., 2014; Tanaka et al., 2020). This Treg-specific down-modulation of TCR signaling appears to be required for the maintenance of Treg homeostasis, as ZAP-70 overexpression led to TCR stimulation-dependent *in vitro* proliferation in otherwise hypo-proliferative Treg cells. It may also ensure Treg and Tconv cells to possess different thresholds and kinetics in T-cell activation and survival. The down-regulation may physiologically enable Treg cells to avoid activation-induced cell death and better survive than effector Tconv cells at an inflammation site to exert dominant control of the inflammation over Tconv cells. On the other hand, TCR stimulation is required for Treg cells to exert suppressive function; for example, TCR signal activates Foxp3 to repress IL-2 and other cytokines production and up-regulate Treg-suppression-associated molecules such CTLA-4. Thus, TCR signal attenuation due to ZAP-70 anomalies may affect Treg homeostasis as well as Treg-mediated suppression, causing profound dysfunction of peripheral Treg cells.

In contrast with the autoimmune-promoting effects (e.g., self-skewing of TCR repertoire of Tconv cells and Treg cell deficiency/dysfunction) of low TCR signaling, further reduction of TCR signaling intensity was autoimmune-inhibitory, hindering the activation of self-reactive Tconv cells upon self-antigen recognition. This is typically seen

in W163A ZAP-70 mutant mice, which developed autoantibodies and hyper-IgE but no clinically or histologically evident autoimmune disease despite their severe TCR self-skewing and Treg cell deficiency. In addition, several ZAP-70 mutant mice previously reported by others possessed various degrees of T-cell immunodeficiency, hyper-IgE, and autoantibody formation, but rarely developed clinically or histologically evident autoimmune diseases (Negishi et al., 1995; Siggs et al., 2007; Hsu et al., 2009). Similarly in humans, many reported cases of ZAP-70 mutations exhibited T cell immune deficiency and hypofunction, and hyper-IgE in some cases, but mostly failed to develop clinically evident autoimmune disease (Picard et al., 2009; Wang et al., 2010; Sakaguchi et al., 2011). These immunodeficiencies without apparent autoimmunity can be attributed to the location of the mutations. A majority of the mutations in mice and humans are present in the kinase domain of ZAP-70 and therefore severely impair TCR signaling, whereas most mutations causative of autoimmunity are present in the SH2 domain (Sakaguchi et al., 2003; Hsu et al., 2009; Sakaguchi et al., 2011; Chan et al., 2016) and may moderately affect TCR signaling via conformational changes of the domain. The autoimmune-causing genetic anomalies of ZAP-70 thus appear to allow positive selection (and hinders negative selection) of Tconv cells capable of mediating the disease; to enable the autoimmune Tconv cells to be functionally competent; and, further, to render Treg cells deficient in number and/or defective in function to impair suppression of autoimmune Tconv cells. Non-autoimmune anomalies such as hyper-IgE and IBD frequently observed with ZAP-70 mutation in humans and mice could also be attributed to Treg deficiency and resulting activation of Th1 and Th17 cells mediating IBD as excessive immune responses against intestinal commensal bacteria, and Tfh cells promoting IgE production (Uhlig et al., 2018; Wing et al., 2014). Further below this range, severe T-cell immune deficiency due to impaired positive selection of both Tconv and Treg cells would ensue.

Our results with ZAP-70 mutant and Tet-on ZAP mice suggest that genetic anomalies of other TCR-proximal signaling molecules could also evoke similar autoimmune disorders by a common mechanism (i.e., reduction of TCR signaling intensity to within the autoimmune range), providing a general model of autoimmunity due to anomalies/variations in various molecules mediating or controlling TCR signaling (Aguado et al., 2002; Sommers et al., 2002; Bottini & Peterson, 2014; Ohashi et al., 2002; Liston et al., 2008; Holst et al., 2008; Hwang et al., 2012; Deng et al., 2013). For

example, genetic polymorphism of PTPN22, which interacts with ZAP-70 and reduces its activity, might well alter TCR-proximal signaling intensity, affecting Tconv as well as Treg cells, thereby contributing to genetic susceptibility to various autoimmune diseases including RA (Bottini & Peterson, 2014). Genetic anomalies/variations in other TCR-proximal signaling molecules associated with human autoimmune diseases, such as Lck, LAT, or Cbl-b (Hauck et al., 2012; Keller et al., 2016; Janssen et al., 2022), might also similarly affect Tconv and Treg cells, and the balance between the two populations, thereby contributing to autoimmune disease development. In addition, such genetic anomalies/variations can interact with other genes to produce different autoimmune diseases; for example, while autoimmune arthritis predominantly developed in ZAC, SKG, and Tet-on ZAP mice on the BALB/c background, lupus-like systemic autoimmunity was a predominant manifestation in SKG mice on the C57BL/6 background (Matsuo et al., 2019). Our results also provide a model of gene/environment interactions in autoimmune disease. Environmental factors, particularly stimuli of innate immunity, may precipitate autoimmune disease in individuals with a signal anomaly/variation that is barely sufficient by itself to evoke autoimmune disease (Sakaguchi et al., 2003; Yoshitomi et al., 2005; Hashimoto et al., 2010). Moreover, this model of autoimmunity based on a shift in the TCR repertoire towards a high self-reactivity enables characterization of normally deleted pathogenic autoimmune Tconv cells and the self-antigens they recognize, in particular, those ubiquitously expressed self-antigens targeted in systemic autoimmune diseases such as RA (Ito et al., 2014). Lastly, for treating and preventing various T cell-dependent immunological disorders, TCR-proximal signaling molecules can be pharmacologically targeted to differentially control the generation and functions of Tconv and Treg cells (Sakaguchi et al., 2020: Tanaka et al., 2020).

MATERIALS AND METHODS

Mice

All mice were maintained in specific pathogen-free facilities and treated in accordance with the institutional guidelines for animal care at the Institute for Frontier Medical Sciences, Kyoto University, and Immunology Frontier Research Center, Osaka University. The animal experiments were approved by the institutional review boards of Kyoto University and Osaka University. BALB/c and SKG mice were purchased from CLEA

Japan. RAG2$^{-/-}$ BALB/c mice were a gift from Y. Shinkai (1992). SKG (Sakaguchi et al., 2003), FIG (Foxp3-IRES-GFP knock-in) (Ohkura et al., 2012), IL-17A KO (Nakae et al., 2002), rtTA Tg (Legname et al., 2000), and Ld-nOVA^{+} DO11.10^{+} RAG2$^{-/-}$ (Kawahata et al., 2002) mice were previously described. H165A (ZAC) and W163A mutant ZAP-70 knock-in mice were generated by using standard molecular cloning procedures and transfection into BALB/c ES cells. PCR was used to genotype the ZAP-70 mutant knock-in allele (wildtype ~400 bp, knock-in allele ~500 bp amplifications by following primers: Zap-F9883 5'-TGG AAA GTA CAG AGC AAG CAA G, Zap-R10289 5'-CTC TGG AGT CCT TCC AGT TCA C and Zap-neo 5'- TAG TGA GAC GTG GTA CTT CC). SKG, H165A (ZAC) KI, W163A KI, thy1.1 mice were crossed with FIG mice to generate FIG SKG, FIG H165A (ZAC) KI, FIG W163A KI, and FIG thy1.1 mice on BALB/c background. H165A (ZAC) KI mice were also crossed to Ld-nOVA^{+} DO11.10^{+} RAG2$^{-/-}$ to generate Ld-nOVA^{+} DO11.10^{+} RAG2$^{-/-}$ H165A (ZAC) KI or DO11.10^{+} RAG2$^{-/-}$ H165A (ZAC) KI mice. For the construction of Tre-hZAP-EGFP transgenic mice, hZap70 cDNA was subcloned into a Tet reporter construct featuring an upstream tetracycline response element (Tre), a minimal cytomegalovirus (CMV) promoter, an HA-tag, a downstream IRES (internal ribosomal entry site)-EGFP reporter, and polyadenylation (polyA) signals. Fragments were prepared and injected into the pronuclei of fertilized oocytes from (CBA×C57Bl/10) F1 mice. PCR amplification of 172 bp band (hZAP forward primer 5'-CAC CAA GTT TGA CAC GCT CTG G and hZAP reverse primer 5'-TCG TCT CTG AGG ATG AGT CAA CG) indicated the presence of the Tre-hZAP-EGFP transgene. Both Tre-hZAP-EGFP and rtTA transgenic strains were backcrossed to BALB/c mice more than 10 times, and they were crossed to BALB/c ZAP-70$^{-/-}$ mice (Negishi et al., 1995). DO11.10 TCR transgenic mice were also crossed to endogenous ZAP-70-deficient Tet-on ZAP mice. Tet-on ZAP mice were fed with doxycycline (Sigma, St. Louis, MO or Nakalai tesque, Japan) containing food (0.5 or 2.0 mg per gram; prepared by CLEA Japan) to induce the expression of hZap-70. Female Tet-on ZAP mice were used unless otherwise stated. All the mice used in this study were on the BALB/c background or backcrossed to BALB/c strain more than 10 times.

Molecular dynamics simulations

The crystal structure of Zap70 (Hatada et al., 1995) (PDB identifier 2OQ1) was used as the initial structure in Molecular Dynamics (MD) simulations. Implicit solvent simulations using the GB/SA model were carried out using GROMACS (van Der Spoel et al., 2005) with the Amber99 force field (Case et al., 2004). Ten independent 40ns simulations for each system using an NVT ensemble at 300K with a step size of 1fs were performed, and snapshots were collected every 10ps. Harmonic distance restraints were applied to the two SH2 domains (residues 10-102 and 166-254, respectively) with a force constant of 2.5 $kJ \cdot mol^{-1} \cdot nm^{-2}$. Dihedral restraints were applied to the linker (residues 114-156). D_I quantified the average distance between the phosphate group of the phospho-tyrosine residue (pY15) on CD3ζ fragment and ZAP-70 inter-SH2 binding residues, Arg17 (NH2), Arg37 (NH1), Tyr238 (CE1), Lys242 (NZ). D_C quantified the average distance between the phosphate group of the phospho-tyrosine residue (pY4) on CD3ζ fragment and ZAP-70 C-terminal SH2 binding residues, Arg170 (NH1), Arg190 (NH2), and Arg192 (NH1). Hydrogen bond analysis was carried out by the VMD package (Humphery et al., 1996) with H-bond cut off length of 3.5 angstrom. Explicit water MD simulations using the TIP3P model were performed by the MyPresto/cosgene package (Fukunishi et al., 2003). A cubic water box containing 13950 water molecules was used. A 100ps simulation using an NPT ensemble with positional restraints on the protein was performed to equilibrate the system; subsequently, the SHAKE algorithm was applied, and the step size was increased to 2 fs. Three 15 ns simulations using an NVT ensemble were performed with snapshots collected every 2 ps.

BIACORE affinity assay

Recombinant SH2 region of ZAP-70 was expressed as GST fusion protein using pGEX4T-3 vector (GE Healthcare) and cleaved with thrombine. Biotinylated ITAM-1 motif of CD3ζ with phosphorylated tyrosine was synthesized and immobilized onto a gold film coated with streptavidin and the affinity was measured by BIACORE 3000 (GE Healthcare). The affinity of an interaction was determined from kinetic measurements, and the equilibrium constant K_D was the ratio of the kinetic rate constants, k_d/k_a.

Cellular analyses by Flow-cytometry

For FACS analyses and cell sorting, the following anti-mouse antibodies were used. Anti-CD25 (PC61)-PE (BD; 553866), anti-CD25(7D4)-V450 (BD; 561257), anti-CD4 (RM4-4)-Biotin (Biolegend; 116010), anti-CD4(RM4-4)-FITC (Biolegend; 116003), anti-CD16/32 (2.4G2)(BD; 553142), anti-CD40L (MR1)-PE (BD; 553658), anti-CD62L (MEL-14)-APC (BD; 553152), anti-CD45RB (16A)-FITC (BD; 553099;), anti-CD44 (IM7)-PE-Cy7 (BD; 560569), anti-CD69 (H1.2F3)-APC (BD; 560689), anti-CTLA-4 (UC10-4F10-11)-PE (BD; 553720), anti-CD103 (M290)-FITC (BD; 557494), anti-CXCR3 (173)-APC (eBioscience; 17-1831-82), anti-CXCR4 (2B11)-PE (eBioscience; 12-9991-82), anti-PD-1 (J43)-FITC (eBioscience; 11-9985-85), anti-Tim-3 (RMT3-23)-APC (eBioscience; 17-5870-80), anti-CD24 (M1/69)-eF450 (eBioscience; 48-0242-80), anti-CD5 (53-7.3)-PE (BD Biosciences; 553022), anti-CD8 (53-6.7)-Biotin (Biolegend; 100704), anti-FR4 (12A5)-APC (BD; 560318), anti-Vβ3 (KJ25)-PE (BD; 553209), anti-Vβ5.1 5.2 (MR9-4)-PE (BD; 553190), anti-Vβ6 (RR4-7)-PE (BD; 553194), anti-Vβ7 (TR310)-PE (BD; 553216), anti-Vβ8.1/8.2 (MR5-2)-PE (BD; 553186), anti-Vβ10 (B21.5)-PE (eBioscience; 12-5805-81), anti-Vβ11 (RR3-15)-PE (BD; 553198), anti-TCR-β (H57-597)-APC (Biolegend; 109212), anti-DO11.10 TCR (KJ1.26)-APC (eBioscience; 17-5808-80), anti-IL-6 (MP5-20F3)-PE (eBioscience; 12-7061-71), anti-IL-4 (11B11)-PE (eBioscience; 12-7041-71), anti-IL-2 (JES6-5H4)-PE (eBioscience; 12-7021-71), anti-IFN-γ (XMG1.2)-eF450 (eBioscience; 48-7311-82), anti-IL-17A (TC11-18H10.1)-BV421 (Biolegend; 506926), anti-IL17F (18F10)-PE (eBioscience; 12-7471-80), anti-Foxp3 (MF23)-AF488 (BD; 560403), anti-Foxp3 (FJK-16s)-PE (eBioscience; 12-5773-82), anti-Helios (22F6)-eF450 (eBioscience; 48-9883-41), anti-CD304 (Neuropilin-1)-biotin (Biolegend; 145213), anti-Nur77 (12.14)-PE (eBioscience; A18533), anti-phospho-p44/42 MAPK (Erk1/2) (197G2) (Cell Signaling Technology; 4377), anti-mouse/human Ki-67 (MKI67)-PE (BD; 556027), anti-GITR (DTA1)-BV421 (BD; 563391), anti-ZAP-70 (1E7.2)-PE (eBioscience; 8012-6695-120), anti-CD3e (145-2C11)-Biotin (BD; 553060), anti-CD25 mAb (7D4)-PE (BD; 558642), anti-Lck (3A5) (Santa Cruz Biotechnology; sc-433), anti-phospho-Src Family (Tyr416) (Cell Signaling Technology; 2101).

For intracellular staining, cells were stained with LIVE/DEAD Fixable Near-IR stain kit (ThermoFisher) or 7-AAD viability dye (Beckman Coulter) before fixation. For Foxp3, CTLA-4, and Ki67 staining, cells were fixed and permeabilized with Mouse Foxp3 Staining Buffer set (eBioscience). For intracellular ZAP-70 analysis, cells were fixed and

permeabilized with BD Cytofix/Cytoperm (BD Biosciences), and stained with anti-ZAP-70-PE (1E7.2) antibody. For intracellular cytokine staining, lymph node or spleen cells were cultured in complete RPMI medium, stimulated with 20 ng/ml PMA and 1 μM ionomycin in the presence of Golgi-Stop (BD Biosciences) for 5 hours. Then, cells were stained with anti-CD4 antibody, permeabilized with BD Cytofix/Cytoperm (BD Biosciences), and stained with anti-cytokine antibodies. Cells were analyzed by FACSCanto II, FACSCalibur, or LSRFortessa (BD Biosciences). Cells were sorted by FACSAria II, FACSAria SORP (BD Biosciences) or MoFlo (Beckman Coulter). Data were analyzed by FlowJo software (Tree Star, OR).

Preparation of T cell sub-populations for cell transfer.

To enrich $CD4^+$ T cells, spleen and lymph node cells were treated with anti-CD8 (3.155) and anti-CD24 (J11d) mAbs and incubated at 37℃ for 30 min on plastic dishes pre-coated with goat anti-rat IgG. Non-adherent cells were stained with anti-CD25 mAb (7D4) and anti-CD4 mAb. Alternatively, $Foxp3^+$ $CD4^+$ Treg cells were purified from FIG BALB/c WT (thy1.1 or thy1.2), FIG ZAC, FIG SKG, or FIG W163A mice based on GFP expression. $CD4^+$ whole, $CD4^+CD25^-$ T, $CD4^+CD25^+$ Treg or $Foxp3^+$ $CD4^+$ Treg cells were purified by MoFlo Cytometer (DakoCytomation, CA, USA) with >96% purity. $CD4^+$ whole, $CD4^+$ $CD25^-$ T cells, or CD4SP $TCR\beta^{high}$ thymocytes ($3x10^5$, $5\ x10^5$, or $1x10^6$, as indicated) were i.v. injected into recipient mice.

Single-cell RNA sequencing of transcriptome and TCR

Single cell- encapsulation, barcoding and sequencing. $CD4^+$ $Foxp3^-$ or $Foxp3^+$ cells from FIG BALB/c WT or FIG ZAC BALB/c mice were collected by FACSAria SORP (BD Biosciences). Cells from inflamed joint, draining popliteal lymph node (dLN), and spleen of each FIG ZAC mice were barcoded with TotalSeq hashtag (BioLegend) antibodies and processed with Chromium Single Cell 5' Library & Gel bead kit (10x Genomics) and loaded onto a Chromium Single Cell Chip (10x Genomics) according to manufacturer's instructions. A maximum of 10,000 cells per sample was targeted to generate TCR VDJ and Gene expression libraries. HiSeq3000 and NovaSeq6000 were used for sequencing.

Pre-processing of single cell RNA-seq data. FASTQ files were aligned to the mouse reference genome (GRCm38, and GRCm38 VDJ v5.0.0, from 10x Genomics), filtered and

counted for barcode and unique molecular identifiers (UMIs) by the 10x Genomics software Cell Ranger v.5.0. Except where specified, all single cell data was analyzed by Seurat v4.0 R package (Hao et al., 2021; Stoeckius et al., 2018). Hashtag demultiplexing was performed by the method integrated in Seurat and number of single cells was normalized among spleen cell samples. Using normalized UMI counts, the top 2,000 variable genes were identified in each batch independently, all batches matrices were merged and the combined variable features of each batch were scaled. Batch correction and data integration was performed by the R package Canek (Loza et al., 2022), which uses a mutual nearest neighbors (MNNs) approach combined with a hybrid linear/nonlinear framework to correct cell type specific batch effects. Data quality control was next performed in the integrated gene expression matrix: cells with less than 200 (poor quality reads) or more than 2500 expressed genes (doublets) and/or more than 5% of mitochondrial counts (damaged and dead cells) were removed. A total number of 12,961 cells were retained from which 7,073 cells correspond to WT mice and 5,888 to ZAC mice, and used for further analyses.

Identification of cell clusters. The identification of cell clusters based on gene expression data was performed in the integrated data set by Seurat v4.0. Cells lacking *CD3D*, *CD3E* and *CD3G* expression were removed. The uniform manifold approximation and projection (UMAP) was used to visualize gene expression profiles and clusters.

Pseudotime analysis. Monocle 3 (Trapnell et al., 2014) method was applied on the Tconv dataset to perform a single-cell trajectory analysis. Cells expressing high levels of naïve T cell markers (*CCR7*, *SELL* and *IL7R*) were set as origin for an unsupervised algorithm for temporally ordering individual cells according to the sequence of gene expression changes without the need of known markers.

T cell repertoire analysis. TCR information was obtained from Cell Ranger all_contig_annotations.csv output file and filtered to remove low quality and unproductive sequences, as well as putative doublets (barcodes associated with more than one alpha and beta chains). Repertoire diversity and clonality in each gene expression cluster was examined by means of the inverse Simpson's Diversity index. Clonotype tracking across Th17 cells in spleen and tissues of ZAC mice was performed by the Immunarch R package v0.6.6 (ImmunoMind Team, 2019). Top clonotype overlaps and gene usage analysis were examined by customized R code.

Cell proliferation and Suppression assay.

RPMI 1640 medium supplemented with 10% FBS, 50μM 2-ME, 100 IU/ml penicillin, and 100μg/ml streptomycin (Nacalai Tesque), and 10mM HEPES buffer was used for T cell culture. $CD4^+CD25^-$ T cells ($2.5x10^4$) were incubated in round-bottom 96-well plates with $5.0x10^4$ irradiated splenocytes and 0.5μg/ml soluble anti-CD3 (2C11). In suppression assays (Takahashi et al., 1998), responder T cells (Tresp; $CD25^-CD4^+$ or $Foxp3^-$ $CD25^-$ $CD4^+$ splenic T cells), irradiated splenocytes, and indicated ratios of Treg cells ($Foxp3^+$ $CD4^+$ Treg or $CD25^{high}$ $CD4^+$ splenic T cells) were used. Graded concentrations of doxycycline were added in indicated experiments. 3H-thymidine (Perkin Elmer) incorporation was measured for the last 8 hours of 72-hour incubation.

ELISA

Anti-parietal cell antibody and RF titers were assessed by ELISA as previously described (Sakaguchi et al., 2003; Takahashi et al., 1998). Anti-CCP antibody was assessed by MESACUP-2 CCP kit using anti-mouse Ig antibody (MBL). Serum IgG, IgG1, and IgG2a levels were measured by ELISA using either Mouse IgG ELISA Quantitation Kit (Bethyl Laboratories) or Clonotyping Elisa kits (Southern Biotech). IgE levels were measured by OptEIA Mouse IgE ELISA set (BD Biosciences).

Western blotting

Sorted cells were treated with NP-40 buffer (1% NonidetP-40, 20 mM Tris pH 7.8, 150 mM NaCl, 2 mM $MgCl_2$), supplemented with the protease inhibitors phenylmethylsulfonylfluoride (PMSF, 1 mM) and CLAP (5 μg/ml each of chymostatin, pepstatin A, antipain hydrochloride and 10 μg/ml leupeptin hemisulphate) and a phosphatase inhibitor cocktail (Roche), and subsequently with Laemmli buffer. Lysates from 1 x 10^5 cells from each sample were run on 7.5% polyacrylamide gel or 12-230kDa capillary with total protein normalization on Jess (Proteinsimple) with anti-phospho-Src family (Y416) antibody (Cell Signaling Technology) for detection. Analysis was performed by LAS-4000 (Fujifilm) or Jess (Proteinsimple).

Quantitative PCR

From sorted T cells, RNA was isolated with RNeasy Mini Kit (Qiagen) and cDNA was synthesized with SuperScript III reverse transcriptase kit (Invitrogen). Quantitative real-time PCR was performed by TaqMan probe Mm00445259_m1 covering IL-4 gene using Step-OnePlus real-time PCR system (Applied biosystems, Life Technologies) according to the instruction provided by the manufacturer.

Foxp3 bound TCR signalling genes

Foxp3 binding peaks were identified from ChIPseq database from Morikawa et al (2014). Foxp3-bound TCR signalling genes were defined using Foxp3 ChIP-seq databases from Samstein et al (2012) and Kitagawa et al (2017). For each ChIP-seq experiments, peaks were identified by findPeaks in Homer program (version 4.7.2)(Fejes et al., 2008) and regions commonly detected in two ChIP-seq experiments were considered as reliable Foxp3 binding sites. Genes with Foxp3 binding at their promoter (2.5 kb upstream of transcription start sites) were selected as Foxp3 target genes.

Clinical assessment of arthritis

Joint swelling was monitored by inspection and scored as follows: 0, no joint swelling; 0.1, swelling of one finger joint; 0.5, mild swelling of wrist or ankle; and 1.0, severe swelling of wrist or ankle. Scores for all fingers and toes, wrists, and ankles were totaled for each mouse (Sakaguchi et al., 2003).

Histological assessments of pathology

Organs were fixed in buffered 10% formalin, paraffin-embedded, and sections were stained with hematoxylin and eosin (HE). Histological scoring was performed on HE-stained tissue sections. Each HE-stained tissue section (synovium, muscle, lung, skin, and colon) was given an inflammation severity score based on the published criteria (Sather et al., 2007; Wooley et al., 1981; Okiyama et al., 2009; Sheil et al., 2004). Histological severity of inflammation or histological changes in each tissue was graded on a scale of 0, no inflammation or changes, 1, minimal, 2, mild, 3, moderated and 4, marked inflammation or changes in a blinded fashion. Sections of 6μm thickness were cut along a longitudinal axis for scoring of synovitis. Severity of mononuclear cell infiltration in synovium, synovial tissue thickening, and pannus formation were examined, separately.

HE-sections of the proximal muscles (hamstrings and quadriceps) and crural muscles were examined for the presence of mononuclear cell infiltration and degeneration of muscle fibers. For the lung, perivascular, peribronchial, and alveolar inflammation were scored separately. For the skin, inflammation in the dermal, epidermis, and epidermal changes such as hyperkeratosis or ulceration were considered separately. For colitis, stool consistency with diarrhea score of 2, liquid brown, or higher was monitored as a preliminary indication, and inflammatory changes of proximal (ascending and transverse colon) and distal colon (descending colon) by histology were also graded separately in a blinded fashion. Histological severities of colitis were according to the published criteria (Asseman et al., 1999). Briefly, grade 0, no changes, 1, minimal cell infiltrates, 2, mild scattered to diffuse inflammatory cell infiltrates, with mild epithelial hyperplasia, 3, moderate inflammatory cell infiltrate with moderate epithelial hyperplasia and mucin depletion, 4, marked inflammatory cell infiltrates associated with ulceration. Total histological score was computed by summing these inflammation subscores. Ranges of possible scores for each tissue were as follows: synovium, 0-12, muscle, 0-8, lung, 0-12, skin, 0-12, and colon, 0-8.

Statistical analyses

Statistical analyses were performed using Prism software (GraphPad) unless otherwise described. Two-tailed unpaired Student's t test, Spearman rank correlation test, Logrank test, Fisher's exact test, F-test, or Mann-Whitney U test were used where appropriate. Refer to figure legends for the statistical tests used in each experiment.

Online supplemental material

Fig. S1 shows molecular dynamics of ZAP-70 mutants and generation of ZAP-70 mutation knock-in mice. Fig. S2 shows highly activated and inflammatory phenotypes of ZAC Tconv and Treg cells with impaired Treg function. Fig. S3 show clonal expansion of Th17-like cluster and Treg cells in ZAC mice. Fig. S4 shows altered development and self-skewed TCR repertoire selection in the thymus of ZAP-70 mutant mice. Fig. S5 shows Dox dose dependent expression of ZAP-70 and elicitation of autoimmune diseases in Dox-low Tet-on ZAP mice. Table S1 details TCR clonotypes of ZAC Tconv and Treg cells. Video S1-S4 show molecular dynamics simulations of WT or mutant ZAP-70.

Data availability

Raw and processed data files for the scRNA-seq analysis have been deposited in the DDBJ Sequence Read Archive database (accession number DRA010311) and NCBI Gene Expression Omnibus (accession number GSE180432). All other data that support the findings of this study are available from the corresponding author upon request.

ACKNOWLEDGMENTS

We thank R. Ishii, M. Tanaka, Y. Qian, M. Matsushita, M. Yoshida, M. Matsuura, H. Watanabe, G. Kondo, and the NGS core facility of the Research Institute for Microbial Diseases, Osaka University for technical support; J.T. White for critical reading of the manuscript; our lab members for valuable discussions; This work was supported by JSPS grants-in-aid 26860331, 17K15723, 22H02920 (to A.T.), 20K16286 (to M.A.L.C.), 19K16692 (to E.L.L.) 18H02430 (to D.M.S.), grants-in-aid from the Ministry of Education, Sports, and Culture of Japan 16H06295, 26253030 (to S.S.), Japan Agency for Medical Research and Development BINDS JP21am0101108 (to D.M.S.), CREST 17gm0410016, P-CREATE 18cm0106303, and LEAP 18gm0010005 (to S.S.).

Author contributions: Conceptualization, A.T., S.M., and S.S.; Methodology, A.T., S.M., T.N., S.T., M.A.L.C., L.J.; Investigation, A.T., S.M., T.N., M.A.L.C., S.T., E.L.L., S.A., C.F., K.H., T.M., Y.I., M.H., and R.U.; Software, Formal Analysis, M.A.L.C., L.J., H.M., Y.K., J.H., and D.M.S., Resources, R.Z.; Writing, A.T., S.M., and S.S.; Funding Acquisition, A.T., M.A.L.C., E.L.L., D.M.S., and S.S.; Supervision, A.T., N.S. and S.S.

Disclosures: The authors declare no conflicting financial interests.

REFERENCES

Aguado, E., S. Richelme, S. Nunez-Cruz, A. Miazek, A.M. Mura, M. Richelme, X.J. Guo, D. Sainty, H.T. He, B. Malissen, and M. Malissen. 2002. Induction of T helper type 2 immunity by a point mutation in the LAT adaptor. *Science* 296:2036-2040.

Anderson, G., K.J. Hare, and E.J. Jenkinson. 1999. Positive selection of thymocytes: the long and winding road. *Immunol Today* 20:463-468.

Ashouri, J.F., L. Hsu, S. Yu, D. Rychkov, Y. Chen, D.A. Cheng, M. Sirota, E. Hansen, L. Lattanza, J. Zikherman, and A. Weiss. 2019. Reporters of TCR signaling identify arthritogenic T cells in murine and human autoimmune arthritis. *Proc. Natl. Acad. Sci. U. S. A.* 116:18517–18527.

Asseman, C., S. Mauze, M.W. Leach, R.L. Coffman, and F. Powrie. 1999. An essential role for interleukin 10 in the function of regulatory T cells that inhibit intestinal inflammation. *J Exp Med* 190:995-1004.

Au-Yeung, B.B., N.H. Shah, L. Shen, and A. Weiss. 2018. ZAP-70 in Signaling, Biology, and Disease. *Annu Rev Immunol* 36:127-156.

Bottini, N., and E.J. Peterson. 2014. Tyrosine phosphatase PTPN22: multifunctional regulator of immune signaling, development, and disease. *Annu Rev Immunol* 32:83-119.

Case, D.A., T.A. Darden, T.E. Cheatham, III, C.L. Simmerling, J. Wang, R.E. Duke, R. Luo, K.M. Merz, B. Wang, D.A. Pearlman, M. Crowley, S. Brozell, V. Tsui, H. Gohlke, J. Mongan, V. Hornak, G. Cui, P. Beroza, C. Schafmeister, J.W. Caldwell, W.S. Ross, and P.A. Kollman. 2004. AMBER 8, University of California, San Francisco. 310 pp.

Chan, A.Y., D. Punwani, T.A. Kadlecek, M.J. Cowan, J.L. Olson, E.F. Mathes, U. Sunderam, S.M. Fu, R. Srinivasan, J. Kuriyan, S.E. Brenner, A. Weiss, and J.M. Puck. 2016. A novel human autoimmune syndrome caused by combined hypomorphic and activating mutations in ZAP-70. *J Exp Med* 213:155-165.

Deng, G.M., J. Beltran, C. Chen, C. Terhorst, and G.C. Tsokos. 2013. T cell CD3ζ deficiency enables multiorgan tissue inflammation. *J Immunol* 191:3563-3567.

Elder, M.E., D. Lin, J. Clever, A.C. Chan, T.J. Hope, A. Weiss, and T.G. Parslow. 1994. Human severe combined immunodeficiency due to a defect in ZAP-70, a T cell tyrosine kinase. *Science* 264:1596-1599.

Fejes, A.P., G. Robertson, M. Bilenky, R. Varhol, M. Bainbridge, and S.J. Jones. 2008. FindPeaks 3.1: a tool for identifying areas of enrichment from massively parallel short-read sequencing technology. *Bioinformatics* 24:1729-1730.

Fukunishi, Y., Y. Mikami, and H. Nakamura. 2003. The filling potential method: A method for estimating the free energy surface for protein-ligand docking. *Journal of Physical Chemistry B* 107:13201-13210.

Hao, Y., S. Hao, E. Andersen-Nissen, W.M. Mauck, 3rd, S. Zheng, A. Butler, M.J. Lee, A.J. Wilk, C. Darby, M. Zager, P. Hoffman, M. Stoeckius, E. Papalexi, E.P. Mimitou, J. Jain, A. Srivastava, T. Stuart, L.M. Fleming, B. Yeung, A.J. Rogers, J.M. McElrath, C.A. Blish, R. Gottardo, P. Smibert, and R. Satija. 2021. Integrated analysis of multimodal single-cell data. *Cell* 184:3573-3587 e3529.

Hashimoto, M., K. Hirota, H. Yoshitomi, S. Maeda, S. Teradaira, S. Akizuki, P. Prieto-Martin, T. Nomura, N. Sakaguchi, J. Kohl, B. Heyman, M. Takahashi, T. Fujita, T. Mimori, and S. Sakaguchi. 2010. Complement drives Th17 cell differentiation and triggers autoimmune arthritis. *J Exp Med* 207:1135-1143.

Hatada, M.H., X. Lu, E.R. Laird, J. Green, J.P. Morgenstern, M. Lou, C.S. Marr, T.B. Phillips, M.K. Ram, K. Theriault, and et al. 1995. Molecular basis for interaction of the protein tyrosine kinase ZAP-70 with the T-cell receptor. *Nature* 377:32-38.

Hauck, F., C. Randriamampita, E. Martin, S. Gerart, N. Lambert, A. Lim, J. Soulier, Z. Maciorowski, F. Touzot, D. Moshous, P. Quartier, S. Heritier, S. Blanche, F. Rieux-Laucat, N. Brousse, I. Callebaut, A. Veillette, C. Hivroz, A. Fischer, S. Latour, and C. Picard. 2012. Primary T-cell immunodeficiency with immunodysregulation caused by autosomal recessive LCK deficiency. *J. Allergy Clin. Immunol.* 130:1144-1152.

Herman, A., J.W. Kappler, P. Marrack, and A.M. Pullen. 1991. Superantigens: mechanism of T-cell stimulation and role in immune responses. *Annu Rev Immunol* 9:745-772.

Hirota, K., M. Hashimoto, H. Yoshitomi, S. Tanaka, T. Nomura, T. Yamaguchi, Y. Iwakura, N. Sakaguchi, and S. Sakaguchi. 2007. T cell self-reactivity forms a cytokine milieu for spontaneous development of IL-17^{+} Th cells that cause autoimmune arthritis. *J Exp Med* 204:41-47.

Holst, J., H. Wang, K.D. Eder, C.J. Workman, K.L. Boyd, Z. Baquet, H. Singh, K. Forbes, A. Chruscinski, R. Smeyne, N.S. van Oers, P.J. Utz, and D.A. Vignali. 2008. Scalable signaling mediated by T cell antigen receptor-CD3 ITAMs ensures effective negative selection and prevents autoimmunity. *Nat Immunol* 9:658-666.

Hsu, L.Y., Y.X. Tan, Z. Xiao, M. Malissen, and A. Weiss. 2009. A hypomorphic allele of ZAP-70 reveals a distinct thymic threshold for autoimmune disease versus autoimmune reactivity. *J Exp Med* 206:2527-2541.

Humphrey, W., A. Dalke, and K. Schulten. 1996. VMD: Visual molecular dynamics. *J Mol Graph Model* 14:33-38.

Hwang, S., K.D. Song, R. Lesourne, J. Lee, J. Pinkhasov, L. Li, D. El-Khoury, and P.E. Love. 2012. Reduced TCR signaling potential impairs negative selection but does not result in autoimmune disease. *J Exp Med* 209:1781-1795.

Ito, Y., M. Hashimoto, K. Hirota, N. Ohkura, H. Morikawa, H. Nishikawa, A. Tanaka, M. Furu, H. Ito, T. Fujii, T. Nomura, S. Yamazaki, A. Morita, D.A. Vignali, J.W. Kappler, S. Matsuda, T. Mimori, N. Sakaguchi, and S. Sakaguchi. 2014. Detection of T cell responses to a ubiquitous cellular protein in autoimmune disease. *Science* 346:363-368.

Janssen E, Peters Z, Alosaimi MF, Smith E, Milin E, Stafstrom K, Wallace JG, Platt CD, Chou J, El Ansari YS, Al Farsi T, Ameziane N, Al-Ali R, Calvo M, Rocha ME, Bauer P, Al-Sannaa NA, Al Sukaiti NF, Alangari AA, Bertoli-Avella AM, G.R. 2022. Immune dysregulation caused by homozygous mutations in CBLB. *J. Clin. Invest.* Aug 25:e154487.

Kawahata, K., Y. Misaki, M. Yamauchi, S. Tsunekawa, K. Setoguchi, J. Miyazaki, and K. Yamamoto. 2002. Generation of $CD4^+CD25^+$ regulatory T cells from autoreactive T cells simultaneously with their negative selection in the thymus and from nonautoreactive T cells by endogenous TCR expression. *J Immunol* 168:4399-4405.

Keller, B., I. Zaidman, O.S. Yousefi, D. Hershkovitz, J. Stein, S. Unger, K. Schachtrup, M. Sigvardsson, A.A. Kuperman, A. Shaag, W.W. Schamel, O. Elpeleg, K. Warnatz, and P. Stepensky. 2016. Early onset combined immunodeficiency and autoimmunity in patients with loss-of-function mutation in LAT. *J Exp Med* 213:1185-1199.

Kitagawa, Y., N. Ohkura, Y. Kidani, A. Vandenbon, K. Hirota, R. Kawakami, K. Yasuda, D. Motooka, S. Nakamura, M. Kondo, I. Taniuchi, T. Kohwi-Shigematsu, and S. Sakaguchi. 2017. Guidance of regulatory T cell development by Satb1-dependent super-enhancer establishment. *Nat Immunol* 18:173-183.

Klein, L., E.A. Robey, and C.S. Hsieh. 2019. Central $CD4^+$ T cell tolerance: deletion versus regulatory T cell differentiation. *Nat Rev Immunol* 19:7-18.

Legname, G., B. Seddon, M. Lovatt, P. Tomlinson, N. Sarner, M. Tolaini, K. Williams, T. Norton, D. Kioussis, and R. Zamoyska. 2000. Inducible expression of a p56Lck transgene reveals a central role for Lck in the differentiation of CD4 SP thymocytes. *Immunity* 12:537-546.

Liston, A., A. Enders, and O.M. Siggs. 2008. Unravelling the association of partial T-cell immunodeficiency and immune dysregulation. *Nat Rev Immunol* 8:545-558.

Loza, M., S. Teraguchi, D.M. Standley, and D. Diez. 2022. Unbiased integration of single cell transcriptome replicates. *NAR Genom Bioinform* 4:lqac022.

Matsuo, T., M. Hashimoto, S. Sakaguchi, N. Sakaguchi, Y. Ito, M. Hikida, T. Tsuruyama, K. Sakai, H. Yokoi, M. Shirakashi, M. Tanaka, H. Ito, H. Yoshifuji, K. Ohmura, T. Fujii, and T. Mimori. 2019. Strain-Specific Manifestation of Lupus-like Systemic Autoimmunity Caused by Zap70 Mutation. *J Immunol* 202:3161-3172.

Morikawa, H., N. Ohkura, A. Vandenbon, M. Itoh, S. Nagao-Sato, H. Kawaji, T. Lassmann, P. Carninci, Y. Hayashizaki, A.R. Forrest, D.M. Standley, H. Date, S. Sakaguchi, and F. Consortium. 2014. Differential roles of epigenetic changes and Foxp3 expression in regulatory T cell-specific transcriptional regulation. *Proc Natl Acad Sci U S A* 111:5289-5294.

Nakae, S., Y. Komiyama, A. Nambu, K. Sudo, M. Iwase, I. Homma, K. Sekikawa, M. Asano, and Y. Iwakura. 2002. Antigen-specific T cell sensitization is impaired in IL-17-deficient mice, causing suppression of allergic cellular and humoral responses. *Immunity* 17:375-387.

Nazarov V, Tsvetkov V, Rumynskiy E, Popov A, Balashov I, Samokhina M. 2019. immunarch: Bioinformatics Analysis of T-Cell and B-Cell Immune Repertoires. Zenodo. https://immunarch.com/

Negishi, I., N. Motoyama, K. Nakayama, K. Nakayama, S. Senju, S. Hatakeyama, Q. Zhang, A.C. Chan, and D.Y. Loh. 1995. Essential role for ZAP-70 in both positive and negative selection of thymocytes. *Nature* 376:435-438.

Ohashi, P.S. 2002. T-cell signalling and autoimmunity: molecular mechanisms of disease. *Nat Rev Immunol* 2:427-438.

Ohkura, N., M. Hamaguchi, H. Morikawa, K. Sugimura, A. Tanaka, Y. Ito, M. Osaki, Y. Tanaka, R. Yamashita, N. Nakano, J. Huehn, H.J. Fehling, T. Sparwasser, K. Nakai, and S. Sakaguchi. 2012. T cell receptor stimulation-induced epigenetic changes and Foxp3 expression are independent and complementary events required for Treg cell development. *Immunity* 37:785-799.

Okiyama, N., T. Sugihara, Y. Iwakura, H. Yokozeki, N. Miyasaka, and H. Kohsaka. 2009. Therapeutic effects of interleukin-6 blockade in a murine model of polymyositis that does not require interleukin-17A. *Arthritis Rheum* 60:2505-2512.

Picard, C., S. Dogniaux, K. Chemin, Z. Maciorowski, A. Lim, F. Mazerolles, F. Rieux-Laucat, M.C. Stolzenberg, M. Debre, J.P. Magny, F. Le Deist, A. Fischer, and C. Hivroz. 2009. Hypomorphic mutation of ZAP70 in human results in a late onset immunodeficiency and no autoimmunity. *Eur J Immunol* 39:1966-1976.

Sakaguchi, N., T. Takahashi, H. Hata, T. Nomura, T. Tagami, S. Yamazaki, T. Sakihama, T. Matsutani, I. Negishi, S. Nakatsuru, and S. Sakaguchi. 2003. Altered thymic T-cell selection due to a mutation of the ZAP-70 gene causes autoimmune arthritis in mice. *Nature* 426:454-460.

Sakaguchi, S., K. Fukuma, K. Kuribayashi, and T. Masuda. 1985. Organ-specific autoimmune diseases induced in mice by elimination of T cell subset. I. Evidence for the active participation of T cells in natural self-tolerance; deficit of a T cell subset as a possible cause of autoimmune disease. *J. Exp. Med.* 161:72–87.

Sakaguchi, S., N. Sakaguchi, M. Asano, M. Itoh, and M. Toda. 1995. Immunologic self-tolerance maintained by activated T cells expressing IL-2 receptor alpha-chains (CD25). Breakdown of a single mechanism of self-tolerance causes various autoimmune diseases. *J Immunol* 155:1151-1164.

Sakaguchi, S., S. Tanaka, A. Tanaka, Y. Ito, S. Maeda, N. Sakaguchi, and M. Hashimoto. 2011. Thymus, innate immunity and autoimmune arthritis: interplay of gene and environment. *FEBS Lett* 585:3633-3639.

Sakaguchi, S., N. Mikami, J.B. Wing, A. Tanaka, K. Ichiyama, and N. Ohkura. 2020. Regulatory T Cells and Human Disease. *Annu Rev Immunol* 38:541-566.

Samstein, R.M., A. Arvey, S.Z. Josefowicz, X. Peng, A. Reynolds, R. Sandstrom, S. Neph, P. Sabo, J.M. Kim, W. Liao, M.O. Li, C. Leslie, J.A. Stamatoyannopoulos, and A.Y. Rudensky. 2012. Foxp3 exploits a pre-existent enhancer landscape for regulatory T cell lineage specification. *Cell* 151:153-166.

Sather, B.D., P. Treuting, N. Perdue, M. Miazgowicz, J.D. Fontenot, A.Y. Rudensky, and D.J. Campbell. 2007. Altering the distribution of Foxp3^{+} regulatory T cells results in tissue-specific inflammatory disease. *J Exp Med* 204:1335-1347.

Schrum, A.G., L.A. Turka, and E. Palmer. 2003. Surface T-cell antigen receptor expression and availability for long-term antigenic signaling. *Immunol Rev* 196:7-24.

Sheil, B., J. McCarthy, L. O'Mahony, M.W. Bennett, P. Ryan, J.J. Fitzgibbon, B. Kiely, J.K. Collins, and F. Shanahan. 2004. Is the mucosal route of administration essential for

probiotic function? Subcutaneous administration is associated with attenuation of murine colitis and arthritis. *Gut* 53:694-700.

Shinkai, Y., G. Rathbun, K.P. Lam, E.M. Oltz, V. Stewart, M. Mendelsohn, J. Charron, M. Datta, F. Young, A.M. Stall, and et al. 1992. RAG-2-deficient mice lack mature lymphocytes owing to inability to initiate V(D)J rearrangement. *Cell* 68:855-867.

Siggs, O.M., L.A. Miosge, A.L. Yates, E.M. Kucharska, D. Sheahan, T. Brdicka, A. Weiss, A. Liston, and C.C. Goodnow. 2007. Opposing functions of the T cell receptor kinase ZAP-70 in immunity and tolerance differentially titrate in response to nucleotide substitutions. *Immunity* 27:912-926.

Sommers, C.L., C.S. Park, J. Lee, C. Feng, C.L. Fuller, A. Grinberg, J.A. Hildebrand, E. Lacana, R.K. Menon, E.W. Shores, L.E. Samelson, and P.E. Love. 2002. A LAT mutation that inhibits T cell development yet induces lymphoproliferation. *Science* 296:2040-2043.

Stoeckius, M., S. Zheng, B. Houck-Loomis, S. Hao, B.Z. Yeung, W.M. Mauck, 3rd, P. Smibert, and R. Satija. 2018. Cell Hashing with barcoded antibodies enables multiplexing and doublet detection for single cell genomics. *Genome Biol* 19:224.

Svensson, M.N., K.M. Doody, B.J. Schmiedel, S. Bhattacharyya, B. Panwar, F. Wiede, S. Yang, E. Santelli, D.J. Wu, C. Sacchetti, R. Gujar, G. Seumois, W.B. Kiosses, I. Aubry, G. Kim, P. Mydel, S. Sakaguchi, M. Kronenberg, T. Tiganis, M.L. Tremblay, F. Ay, P. Vijayanand, and N. Bottini. 2019. Reduced expression of phosphatase PTPN2 promotes pathogenic conversion of Tregs in autoimmunity. *J Clin Invest* 129:1193-1210.

Takahashi, T., Y. Kuniyasu, M. Toda, N. Sakaguchi, M. Itoh, M. Iwata, J. Shimizu, and S. Sakaguchi. 1998. Immunologic self-tolerance maintained by $CD25^{+}CD4^{+}$ naturally anergic and suppressive T cells: induction of autoimmune disease by breaking their anergic/suppressive state. *Int Immunol* 10:1969-1980.

Tanaka, A., H. Nishikawa, S. Noguchi, D. Sugiyama, H. Morikawa, Y. Takeuchi, D. Ha, N. Shigeta, T. Kitawaki, Y. Maeda, T. Saito, Y. Shinohara, Y. Kameoka, K. Iwaisako, F. Monma, K. Ohishi, J. Karbach, E. Jager, K. Sawada, N. Katayama, N. Takahashi, and S. Sakaguchi. 2020. Tyrosine kinase inhibitor imatinib augments tumor immunity by depleting effector regulatory T cells. *J Exp Med* 217:

Tanaka, S., S. Maeda, M. Hashimoto, C. Fujimori, Y. Ito, S. Teradaira, K. Hirota, H. Yoshitomi, T. Katakai, A. Shimizu, T. Nomura, N. Sakaguchi, and S. Sakaguchi. 2010. Graded attenuation of TCR signaling elicits distinct autoimmune diseases by altering thymic T cell selection and regulatory T cell function. *J Immunol* 185:2295-2305.

Thornton, A.M., and E.M. Shevach. 1998. $CD4^{+}CD25^{+}$ immunoregulatory T cells suppress polyclonal T cell activation in vitro by inhibiting interleukin 2 production. *J Exp Med* 188:287-296.

Trapnell, C., D. Cacchiarelli, J. Grimsby, P. Pokharel, S. Li, M. Morse, N.J. Lennon, K.J. Livak, T.S. Mikkelsen, and J.L. Rinn. 2014. The dynamics and regulators of cell fate decisions are revealed by pseudotemporal ordering of single cells. *Nat Biotechnol* 32:381-386.

Uhlig, H.H., and F. Powrie. 2018. Translating Immunology into Therapeutic Concepts for Inflammatory Bowel Disease. *Annu Rev Immunol* 36:755-781.

Van Der Spoel, D., E. Lindahl, B. Hess, G. Groenhof, A.E. Mark, and H.J. Berendsen. 2005. GROMACS: fast, flexible, and free. *J Comput Chem* 26:1701-1718.

Wang, H., T.A. Kadlecek, B.B. Au-Yeung, H.E. Goodfellow, L.Y. Hsu, T.S. Freedman, and A. Weiss. 2010. ZAP-70: an essential kinase in T-cell signaling. *Cold Spring Harb Perspect Biol* 2:a002279.

Wing, J.B., W. Ise, T. Kurosaki, and S. Sakaguchi. 2014. Regulatory T cells control antigen-specific expansion of Tfh cell number and humoral immune responses via the coreceptor CTLA-4. *Immunity* 41:1013-1025.

Wooley, P.H., H.S. Luthra, J.M. Stuart, and C.S. David. 1981. Type-Ii Collagen-Induced Arthritis in Mice .1. Major Histocompatibility Complex (I Region) Linkage and Antibody Correlates. *Journal of Experimental Medicine* 154:688-700.

Yoshitomi, H., N. Sakaguchi, K. Kobayashi, G.D. Brown, T. Tagami, T. Sakihama, K. Hirota, S. Tanaka, T. Nomura, I. Miki, S. Gordon, S. Akira, T. Nakamura, and S. Sakaguchi. 2005. A role for fungal β-glucans and their receptor Dectin-1 in the induction of autoimmune arthritis in genetically susceptible mice. *J Exp Med* 201:949-960.

FIGURE LEGENDS

Figure 1. Molecular dynamics of ZAP-70 mutants with reduced affinity for CD3ζ chain.

(A) Structure of ZAP-70 tandem SH2 domains (cyan) and CD3ζ pITAM (red) chain (left), and affinity between CD3ζ phosphorylated ITAM and indicated mutants of ZAP-70 measured by BIACORE (right). Phospho-tyrosine residues (red sticks) of CD3ζ ITAM, phospho-tyrosine binding (PTB) residues (blue sticks) and mutated residues (W163, H165; blue sticks) of ZAP-70 are also shown. Insets show measured distances (dotted lines) between the ITAM phospho-tyrosine (pY15) and the inter-SH2 PTB residues (D_I) and between pY4 and the carboxy-terminal PTB residues (D_C). $K_D = k_d/k_a$. **(B)** Representative snapshots from MD simulations (between 13~18ns) on CD3ζ pITAM (red) and ZAP-70 tandem SH2 domains (blue) with indicated mutations. Phospho-tysosines of CD3ζ and phospho-tyrosine binding (PTB) residues of ZAP-70 are also shown (sticks). See also Video S1-S4. **(C)** Distributions of measured distances between the CD3ζ ITAM phospho-tyrosine (pY15) and the inter-SH2 PTB residues of ZAP-70 (D_I), and between CD3ζ ITAM pY4 and the carboxy-terminal PTB residues of ZAP-70 (D_C). D_I and D_C distances for WT, H165A, W163C, and W163A mutants are shown as log f(D_I, D_C). The boundary of the WT D_I/D_C distribution is indicated with a dotted line.

Figure 2. Spontaneous development of autoimmune diseases in H165A mice. (A-B) Joint swellings of a forepaw and a hindpaw (A) and histology (B) of 21-week-old H165A and BALB/c mice. 200μm scale bars in (B). **(C)** Arthritis incidences (left) and scores (right) for BALB/c, H165A, W163C (SKG), and W163A mice (n=27 each). **(D-E)** Histological (D) and macroscopic views (E) of the colon from H165A and BALB/c mice. Scale bar: 10μm in (D), 10mm in (E). **(F)** Frequency of diarrheic mice in BALB/c and ZAP-70 mutant strains (n=32 each). **(G)** Serum levels of indicated antibodies in BALB/c, SKG, H165A, and W163A mice. **(H)** Arthritis scores after transfer of $1x10^6$ $CD4^+$ T cells from BALB/c, H165A, SKG, or W163A mice into $RAG2^{-/-}$ mice (n=7 each). **(I)** Arthritis scores after mannan treatment of SKG, H165A, W163A, and BALB/c mice. Mean±SD in (C, H-I). Two-tailed unpaired Student's t-test (G). *P<0.05; **P<0.005; ***P<0.0005.

Figure 3. Arthritogenic Th17 cells and impairment of Treg function in ZAC mice. **(A-B)** Frequency of splenic $CD4^+$ and $CD8^+$ T cells (A) and their cell numbers (B) in 8-week-old BALB/c, ZAC, SKG, and W163A mice (top, n=11 each). Frequency of $Foxp3^+$ Treg among $CD4^+$ T cells (bottom, (A) and (B)) or $CD44^{hi}$ $CD4^+$ Tconv cells are also shown (B). **(C)** Representative intracellular cytokine staining of splenic $CD4^+$ T cells from ZAC and BALB/c mice (n=5 each). **(D)** IL-4 mRNA expression levels of freshly isolated splenic $CD4^+$ T cells or $CXCR5^{hi}PD\text{-}1^{hi}$ Tfh cells from Peyer's patches (PP) of ZAC and BALB/c mice. IL-4 expression relative to GAPDH as a reference by qRT-PCR (n=5 each). **(E)** PD-1 and CXCR5 staining of $CD4^+$ T cells from PP of BALB/c and ZAC mice. **(F)** Arthritis scores (left) and frequencies of diarrheic mice (right) in ZAC and IL-$17A^{-/-}$ ZAC mice (n=23 each). **(G)** *In vitro* suppression assay with WT or ZAC $Foxp3^+$ Treg cells with WT $CD4^+$ Tconv at indicated ratios (n=7 each). **(H)** Arthritis scores (left) and frequency of diarrheic mice (right) of ZAC mice intravenously injected with 0.4 or $1.2x10^6$ WT $Foxp3^+$Treg cells at 6 weeks of age (n=7 each). **(I)** Ratios of splenic ZAC and WT Treg cells after 8 weeks of WT Treg transfer as in (H). WT Treg ratio in each chart. **(J)** Arthritis scores of $RAG2^{-/-}$ recipients transferred with $1x10^6$ WT $CD4^+$ T cells, $1x10^6$ ZAC $CD4^+$ T cells, or $1x10^6$ ZAC $CD4^+$ T and $2x10^5$ WT $Foxp3^+$ Treg cells (n=5 each). Mean±SD in (B, D, F-H, J). Two-tailed unpaired Student's t-test in (B, D, G).

Figure 4. Inflammatory Th subsets in ZAC mice by single-cell transcriptomic analysis. **(A)** UMAP visualization of splenic $Foxp3^-CD4^+$ Tconv and $Foxp3^+$ Treg cells from WT or ZAC mice (2 mice each) showing gene expression-based clusters by scRNA-seq. **(B)** Composition of each UMAP clusters by Tconv or Treg cells from WT or ZAC mice. **(C)** Dot plots showing expression levels of Th and Treg signature genes, and composition of WT and ZAC samples in each cluster. **(D)** Expression levels of Th and Treg signature genes.

Figure 5. Clonal expansion of Th17-like cluster and Treg cells infiltrating the inflamed joint of ZAC mice.

(A) TCR repertoire diversity of naïve or effector Tconv and Treg cells from the spleen of WT and ZAC mice in Fig. 4A, expressed as inverse Simpson index. **(B)** TCR counts of top 20 frequent clonotypes in splenic Tconv and Treg cells from two WT and two ZAC

mice (see also Table S1). **(C)** TCR repertoire diversity of each cluster in Fig. 4A, color-coded by predominant composition in each cluster. **(D-E)** TCR clonotype tracking of ZAC Tconv (D) and Treg cells (E) in the spleen, draining lymph node (dLN), and inflamed joint of the same mouse (ZAC mouse #1). Cluster 6 (spleen) is also shown in (D) (see also Fig. S3D-E and Table S1). **(F)** TCR clonotype overlaps between splenic Tconv and Treg cells in WT and ZAC mice (2 mice each). **(G)** ZAC Tconv and Treg cells possessing overlapped TCR clonotypes (red dots) in UMAP clusters shown in Fig. 4A.

Figure 6. Altered thymic selections of Tconv and Treg cells in ZAP-70 mutant mice. **(A-B)** CD4SP and CD8SP thymocytes (top row), and $Foxp3^+$ Treg cells among CD4SP thymocytes (bottom row) in 8-week-old BALB/c or ZAP-70 mutant mice. Frequency (A) and cell numbers of CD4SP and $Foxp3^+$ CD4SP Treg cells (B) (n=11 each). **(C)** TCRβ expression levels of DP thymocytes after TCR stimulation *in vitro*. Data are representative of 7 independent experiments. **(D)** TCR Vβ usage of CD4SP thymocytes in BALB/c and ZAP-70 mutant mice (n=5 each). **(E-F)** Thymic development of CD4SP (top row) and Treg cells (bottom row, gated on CD4SP) in $DO11.10^+$ $RAG2^{-/-}$ or Ld-$nOVA^+$ $DO11.10^+$ $RAG2^{-/-}$ mice on the ZAC or WT background. Representative plots (E) and summary (F) (n=5 each). **(G-H)** Proliferation of splenic $Foxp3^-CD4^+$ Tconv cells from indicated mice cultured with irradiated autologous APCs and anti-CD3 antibody (G) or without anti-CD3 antibody (H) (n=5 each). **(I)** Number of splenic $CD4^+$ T cells in $RAG2^{-/-}$ mice 8 weeks after cell transfer of $5x10^5$ $CD4^+$ T cells from the spleen of ZAP-70 mutant mice (n=5 each). Two-tailed unpaired Student's t-test and mean±SD in (B, D, F-I). *P<0.05; **P<0.005; ***P<0.0005.

Figure 7. Treg-specific physiological regulation of TCR signaling molecules differentially affects Treg and Tconv TCR signaling. **(A)** ZAP-70 and Nur77 levels in $Foxp3^-CD4^+$ Tconv and $Foxp3^+$ Treg cells from ZAC or BALB/c WT mice upon *in vitro* αCD3/αCD28 antibody stimulation for 24 hours. Numbers indicate MFI (n=5). **(B-C)** Foxp3 binding (peaks) to *Zap70* and genes encoding TCR signaling molecules (B), and gene expression levels of TCR signaling molecules by $CD4^+$ Tconv and Treg cells before and after stimulation (C). Expression levels as indicated by tag counts per million (tpm) were analyzed from DeepCAGE database (Morikawa et al. 2014; *Foxp3-bound genes

commonly detected in two ChIPseq databases. The arrows indicate transcription start site and boxes indicate exons in (B). **(D)** Proliferation of $Foxp3^+$ Treg and $Foxp3^-CD4^+$ T cells from WT or $rtTA^+hZAP\text{-}70^+$ mice cultured with αCD3 antibody and 1μg/mL Doxycycline (n=3).

Figure 8. Development of arthritis and other autoimmune diseases in Dox-low Tet-on ZAP mice. **(A-B)** Percent survival of Tet-on ZAP mice treated with Dox 2.0 (Dox-high) or low Dox 0.5 (Dox-low) food. Percent survival in (A) and body weight changes in (B) (n=14 and 13, respectively). Body weight changes of BALB/c and $ZAP\text{-}70^{-/-}$ mice (n=5 each) are also shown in (B). **(C)** Joint swelling of a forepaw and a hind paw in Dox 0.5 Tet-on ZAP or BALB/c mice. **(D)** Incidence (left) and severity (right) of arthritis in Tet-on ZAP mice treated with Dox 2.0 or 0.5 food for 10 weeks. **(E-G)** Incidences of histologically evident autoimmune diseases (E), histology of affected organs (F), and disease scores (G), in Dox 0.5 or 2.0 treated Tet-on ZAP or BALB/c mice. Scale bar: 200μm. **(H)** Serum titers of RF and anti-CCP and serum concentrations of IgG and IgE in Tet-on ZAP mice treated with Dox 2.0 or 0.5 food for 10 weeks, untreated (Dox(-)) $ZAP\text{-}70^{-/-}$, or normal BALB/c mice. **(I)** FACS staining of indicated molecules for splenic $Foxp3^-$ and $Foxp3^+CD4^+$ T cells in Tet-on ZAP mice Dox-treated for 10 weeks. Percentage within gate and MFIs (in parentheses) are indicated. **(J)** Intracellular staining of IL-17A and IFN-γ for $CD4^+$ T cells in Dox-treated Tet-on ZAP mice as in (I). Representative of three independent experiments. Two-tailed unpaired Student's t-test in (D, G-H), Logrank test in (A). Mean±SD in (B, D, G).

Figure 9. Dox dose dependent T-cell development and thymic selection in Tet-on ZAP mice. **(A)** CD4 and CD8 expression by thymocytes from Tet-on ZAP mice treated with Dox 2.0 or Dox 0.5 food for 9 weeks. Total thymocyte numbers above each plot. **(B)** GFP expression in thymocyte subsets from Dox-treated Tet-on ZAP mice as in (A). Shaded area indicates negative control. Representative of more than five experiments. **(C)** Numbers of thymic CD4SP, CD8SP, $Foxp3^+$CD4SP, and total thymocytes (left), and splenic $CD4^+$, $CD8^+$ T cells, or $Foxp3^+CD4^+$ Treg cells (right) from Dox 2.0 or 0.5 Tet-on ZAP mice Dox-treated for 10 weeks (n=10 each). **(D)** Correlation between GFP expression (MFI) and frequency of CD4SP, CD8SP, or $Foxp3^+$/CD4SP $TCR\beta^{hi}$

thymocytes in individual Dox 2.0 or 0.5 Tet-on ZAP mice (n=10 and 12-16, respectively). (**E)** Correlation between GFP MFIs and frequency of indicated TCR $V\beta^+$ CD4SP thymocytes in Tet-on ZAP mice. Each circle indicates individual mice and average ratios in adult BALB/c mice (horizontal bar). **(F)** TCR Vβ subfamily usage by splenic $Foxp3^-$ or $Foxp3^+CD4^+$ T cells (n=4). **(G)** *In vitro* proliferation of splenic $CD4^+$ T cells from Dox 0.5 or 2.0 Tet-on ZAP mice in the presence of αCD3 antibody and indicated Dox concentrations for 3 days (n=6). **(H)** Numbers of splenic $CD4^+$ or $CD8^+$ T cells in $RAG^{-/-}$ mice 8 weeks after the transfer of $5x10^5$ splenic T cells from Tet-on ZAP mice treated with Dox 2.0 or 0.5 food for 8 weeks (n=5). The recipient $RAG^{-/-}$ mice were maintained with Dox 0.5 food. **(I)** *In vitro* suppressive activity of Tet-on ZAP or BALB/c $CD25^{hi}CD4^+$ Treg cells on the proliferation of BALB/c $CD25^-CD4^+$ T cells (Tconv) at various ratios in the presence (black) or absence (white) of Dox (1μg/ml). Proliferation of co-cultured cells was shown as a relative percent of $CD25^-CD4^+$ T cells alone at various Dox concentrations. Representative of three independent experiments. Two-tailed unpaired Student's t test (C, F, H); Spearman rank correlation test (D-E). Mean±SD in (C, F-H).

Figure 10. Reduced ZAP-70 expression in the thymus and functional Treg impairment in the periphery are essential for inducing autoimmunity. **(A-B)** Donor CD4SP $TCR\beta^{hi}$ thymocytes ($3x10^5$) from Dox 2.0 or 0.5-treated Tet-on ZAP mice for 4 weeks were transferred to $RAG2^{-/-}$ mice, then treated with Dox 0.5 food for 12 weeks and assessed for indicated diseases. Correlation between GFP MFIs of donor thymocytes and arthritis severity (A), or the occurrences of indicated diseases in recipient $RAG2^{-/-}$ mice (B). (**C-E**) Adoptive transfer of $CD4^+$ or $CD4^+CD25^-$ splenic T cells ($3x10^5$) from Dox-treated Tet-on ZAP mice into $RAG2^{-/-}$ mice. Percent survival (C), incidence of histologically evident autoimmune diseases (D), and histological scores of autoimmune/inflammatory diseases (E) in $RAG2^{-/-}$ recipient mice 12 weeks after cell transfer. **(F)** $CD4^+$ or $CD4^+CD25^-$ splenic T cells ($3x10^5$) from individual Tet-on ZAP mice treated with either Dox 0.5 (left) or 2.0 (right) food for 5 weeks or whole splenocytes from untreated Dox (-) Tet-on ZAP mice were transferred to $RAG2^{-/-}$ mice, then treated with either Dox 0.5 or 2.0 food for 11-12 weeks and monitored arthritis severity (n=3). **(G)** $CD25^{hi}$ $CD4^+$ T cells ($3x10^5$) from Dox 0.5 Tet-on ZAP or BALB/c mice were transferred to 4-week-old Tet-on ZAP recipient mice 3 days after starting Dox 0.5 food

treatment and monitored arthritis severity. Logrank test in (C), Fisher's exact test in (D), Mann-Whitney U test in (E), two-tailed unpaired Student's t-test in (G). Mean±SD in (E-G).

SUPPLEMENTAL MATERIAL

Supplemental Figure S1-S5.

Supplemental Table S1.

Supplemental Video S1-S4.

Figure S1. Molecular dynamics of ZAP-70 mutants and generation of knock-in mice. **(A-B)** Representative snapshots of ZAP-70 tandem SH2 unit with indicated mutation. Overlay snapshot of ZAP-70 tandem SH2 unit before (red) and after (cyan) 15ns of MD simulations (A). Snapshots of MD simulations showing interactions between ZAP-70 SH2 and CD3ζ pITAM chain (B). See also Video S1-S4. **(C)** Dissociation constants as given by the ratio of unbound to bound CD3ζ/ ZAP-70 conformations in Fig. 1C. F-test for statistical analysis. **(D)** Knock-in mutagenesis strategy. The targeting vector with either W163A or H165A mutation and a neomycin resistance gene flanked by loxP sites was generated for homologous recombination to ZAP-70 locus. PGK neo was subsequently deleted by crossing to a Cre deleter strain. **(E)** Protein levels of ZAP-70 in T cells of ZAC, SKG, W163A, and WT BALB/c mice. **(F)** Incidence of arthritis after 10 weeks of transferring either $CD4^+$ or $CD8^+$ T cells from ZAC, SKG, W163A, and WT BALB/c mice into $RAG2^{-/-}$ mice (n=5 each).

Figure S2. ZAC Tconv and Treg cells exhibit highly activated and inflammatory phenotypes with impaired Treg function.

(A) Cell number of total splenocytes (left) and splenic $Foxp3^+CD4^+$ T cells (right) in 8-week-old BALB/c, SKG, ZAC, and W163A mice (n=11 each). **(B-C)** Representative FACS staining of indicated molecules expressed by splenic $Foxp3^-CD4^+$ T cells (B) and $Foxp3^+CD4^+$ Treg cells (C) from ZAC and BALB/c mice (n=5). **(D)** Representative intracellular cytokine staining of splenic $CD4^+$ T cells from BALB/c, ZAC, and IL-17A KO ZAC mice after PMA/ionomycin stimulation (n=3). (**E**) *In vitro* suppression assay with WT or W163A $Foxp3^+$ Treg cells with indicated WT $CD4^+$ Tconv:Treg ratios (n=7 each). (**F**) Representative plots of splenic ZAC and WT $thy1.1^+$ Treg cells after 8 weeks of WT Treg transfer as in (Fig 3H). See also Fig. 3I. **(G-H)** $RAG2^{-/-}$ mice were transferred with WT $CD4^+$ T cells, ZAC $CD4^+$ T cells, or co-transferred with ZAC $CD4^+$ T cells and WT $Foxp3^+CD4^+$ Treg cells from FIG BALB/c mice as in Fig. 3I. Spleen (right) and

spleen weight (left) after 10 weeks of transfer (G), and frequency of diarrheic mice (H) (n = 5 each). Two-tailed unpaired Student's t-test and mean±SD in (A, E, G).

Figure S3. Clonal expansion of Th17-like cluster and Treg cells in ZAC mice.

(A) UMAP representation of two replicates from splenic Foxp3$^-$CD4$^+$ Tconv and Foxp3$^+$CD4$^+$ Treg cells from Foxp3-IRES-GFP (FIG) WT or FIG ZAC mice (2 mice each) by scRNA-seq. **(B)** Heatmap of top 5 highly expressed genes among differentially expressed genes from Foxp3$^-$ CD4$^+$ Tconv cells (left) or Foxp3$^+$ CD4$^+$ Treg cells (right) in each clusters. **(C)** Pseudotime analysis of WT and ZAC Tconv cells based on gene expressions. Trajectory inferences shown in dotted arrow. **(D-E)** TCR clonotype tracking of ZAC Tconv (D) and Treg cells (E) in the spleen, draining lymph node (dLN), and inflamed joint (ZAC mouse #2; see Table S1 for the indicated clonotypes). Cluster 6 (spleen) is also included in (D). **(F)** Helios expression by Foxp3$^+$ CD4$^+$ Treg cells in RAG2$^{-/-}$ mice 10 weeks after transfer of Foxp3$^-$CD4$^+$ T cells from BALB/c or ZAC mice.

Figure S4. Altered development and self-skewed TCR repertoire selection in the thymus of ZAP-70 mutant mice.

(A) Cell number of total thymocytes, CD8 SP thymocytes, and frequency of Foxp3$^+$ cells in CD4SP thymocytes of 8-week-old BALB/c, SKG, ZAC, and W163A mice (n=11 each). **(B)** TCRβ, CD5, CD69, and HSA expressions by DP and CD4SP thymocytes from BALB/c and ZAP-70 mutant mice. MFI in parentheses (n=3 each). **(C)** TCRVβ usage of splenic CD4$^+$ T cells from ZAC, SKG, W163A, and WT BALB/c mice by FACS analysis (n=5 each). **(D)** TCR Vβ repertoire of splenic Foxp3$^+$ CD4$^+$ Treg cells from BALB/c or ZAC mice (n=7 each). **(E)** Kinetics of ERK phosphorylation upon TCR stimulation in CD4$^+$ T cells from ZAC, SKG, W163A, and BALB/c mice (n=7). **(F-G)** Proliferation of total CD4$^+$ T cells from indicated mice cultured in the presence of irradiated autologous APCs with anti-CD3 antibody (F) or without anti-CD3 antibody (G) (n=5 each). **(H)** Lck protein levels in Foxp3$^-$CD4$^+$ T and Foxp3$^+$ Treg cells in ZAC or WT mice. Numbers indicate MFI (n=5). **(I)** Phosphorylated-tyrosine 394 of Lck (pY394-Lck) in Foxp3$^+$ Treg and Foxp3$^-$CD4$^+$T cells from ZAC or WT mice (n=3). Two-tailed unpaired Student's t-test in (A, C-D, F-G). Mean±SD in (A, C-G).

Figure S5. Dox dose dependent expression of ZAP-70 and elicitation of autoimmune diseases in Dox-low Tet-on ZAP mice.

(A) Scheme of Tet-inducible human wild-type ZAP-70 double transgenic mice. rtTA; reverse tetracycline activator, HA; hemagglutinin, TRE; tetracycline-responsive element, PminCMV; minimum CMV promoter. **(B)** Correlation between %GFP^+ cells among $CD3^+$ splenocytes of $rtTA^+$ $hZAP\text{-}70^+$ mice and Dox concentration in the culture. Representative result of three independent experiments. **(C)** Splenocytes of $rtTA^+$ $hZAP\text{-}70^+$ BALB/c mice with intact endogenous ZAP-70 were cultured with Con A (2μg/ml) for 3 days in the presence of indicated concentrations of Dox. The percentages of GFP^+ cells and their MFIs (in parentheses) for $CD3^+$ T cells were shown. Representative result of three independent experiments. **(D)** Correlation between GFP expression and the amount of ZAP-70 assessed by intracellular staining of both human and mouse ZAP-70 in $CD4^+$ T cells from $rtTA^+$ $hZAP\text{-}70^+$ BALB/c mice by specific mAb. Numbers indicate MFIs. **(E)** Representative photos of the ear and the tail of Tet-on ZAP or BALB/c mice treated with low dose Dox for 5 weeks. Note severe dermatitis in the ear and the tail, and systemic debilitation of the mice. **(F)** FACS staining of indicated molecules for splenic $Foxp3^+$ $CD4^+$ T cells in Tet-on ZAP mice Dox-treated for 10 weeks, as in (Fig. 8I). Percentages of positively stained cells and their MFIs (in parentheses) are also shown. **(G)** TCRβ, Foxp3, and GFP expression in freshly isolated thymocytes from BALB/c and Tet-on ZAP mice Dox-treated for 9 weeks. Shaded area indicates isotype control. Representative data of more than five experiments. **(H)** GFP expression in Dox-treated Tet-on ZAP splenocytes in the mice shown in (G). Representative result of three independent experiments. **(I)** Expression of ZAP-70 in thymocytes, splenic $CD4^+$, and splenic $CD8^+$ T cells, detected by intracellular staining with anti-ZAP-70, in Dox-treated Tet-on ZAP mice (n=3 each, mean±SD). **(J)** Surface expression of TCRβ, CD5, CD69, and HSA(CD24) on DP and CD4SP thymocytes in Tet-on ZAP mice treated with high or low dose Dox as in (G). Percentages of positive cells are shown. Representative result of two independent experiments. **(K)** Relative protein expression levels of ZAP-70 in T cells compared to WT BALB/c.

Table S1. TCR clonotypes of Tconv and Treg cells in ZAC mice.

Top 20 expanded TCR clonotypes of $CD4^+$ Tconv (top) and Treg cells (middle) in the spleen of ZAC mice (2 mice) and their TCR counts are listed. Top 20 clonotypes of draining popliteal lymph node (dLN), or inflamed joint sharing the same TCR clonotypes and their TCR counts are also listed. For ZAC Tconv cells, top 20 clonotypes within cluster #6 of the spleen (Th17-like cluster) are also shown (top). TCR clonotype overlaps between ZAC Tconv and ZAC Treg cells are listed with their TCR counts (10 and 13 TCR clonotypes in ZAC mouse #1 and #2, respectively)(bottom). Top 20 clonotypes in each organ or cluster are highlighted (blue). Clonotype IDs in (Fig. 5D-E, S3D-E) are also shown.

Video S1-S4. Molecular dynamics simulations of ZAP-70 tandem SH2 unit.
Representative MD simulation movies of interactions between ZAP-70 tandem SH2 unit (blue), with or without various mutations, and CD3ζ phosphorylated ITAM chain (red). Wildtype (**Video S1**), W163C SKG mutation (**Video S2**), H165A mutation (**Video S3**), and W163A mutation (**Video S4**). The carboxy-terminal phosphotyrosine binding pocket is shown at the upper right side, and the inter-SH2 phosphotyrosine binding pocket is at the upper central part of the tandem SH2 unit. Some of the residues important for phosphotyrosine bindings are shown in aqua blue.

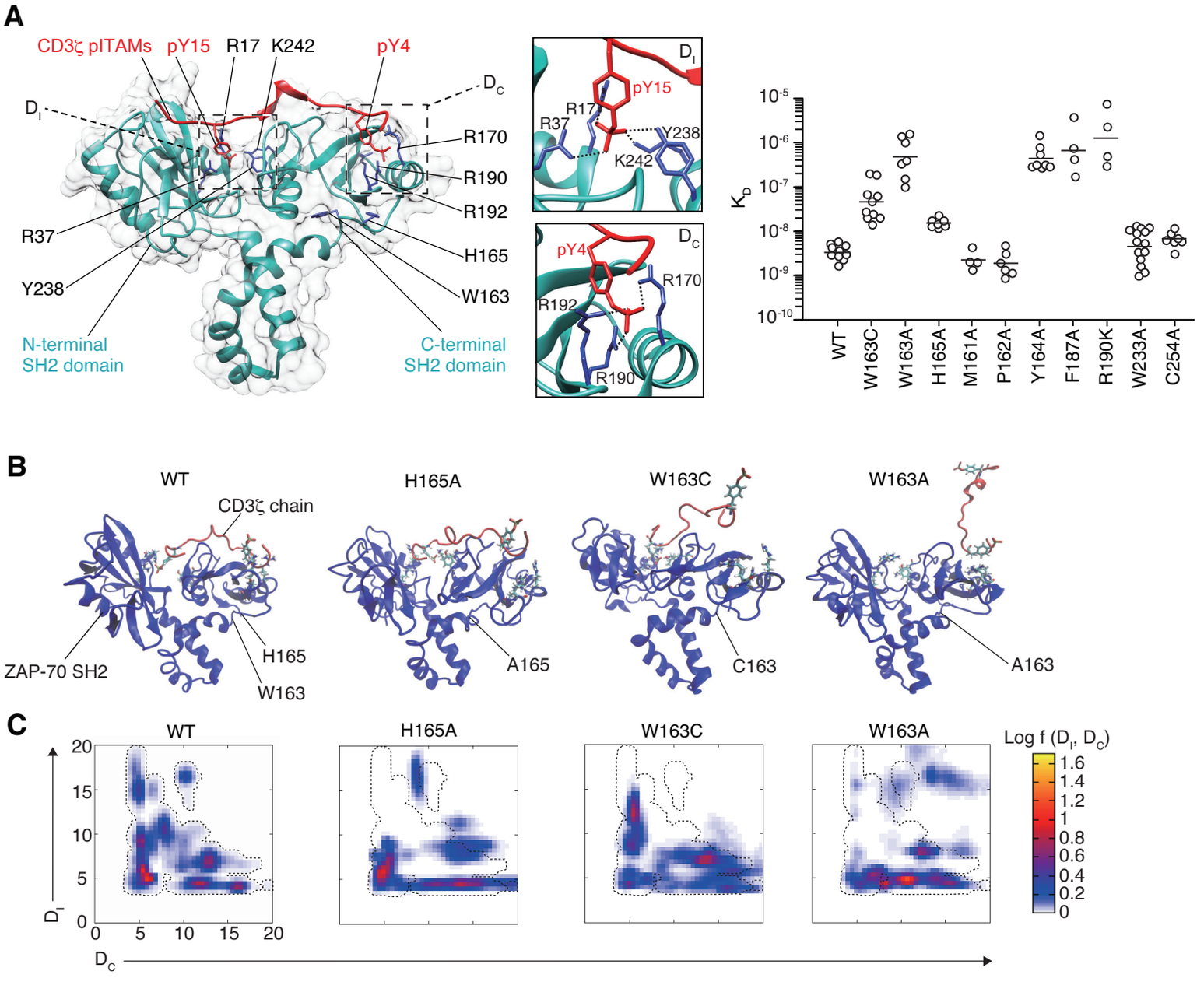
A
CD3ζ pITAMs
pY15
R17
K242
pY4
D_I
D_C
R170
R190
R192
R37
H165
Y238
W163
N-terminal SH2 domain
C-terminal SH2 domain
pY15
R17
R37
Y238
K242
pY4
R170
R192
R190
K_D
WT
W163C
W163A
H165A
M161A
P162A
Y164A
F187A
R190K
W233A
C254A
B
WT
CD3ζ chain
H165A
W163C
W163A
ZAP-70 SH2
H165
W163
A165
C163
A163
C
WT
H165A
W163C
W163A
Log f (D_I, D_C)
D_I
D_C

Figure 1

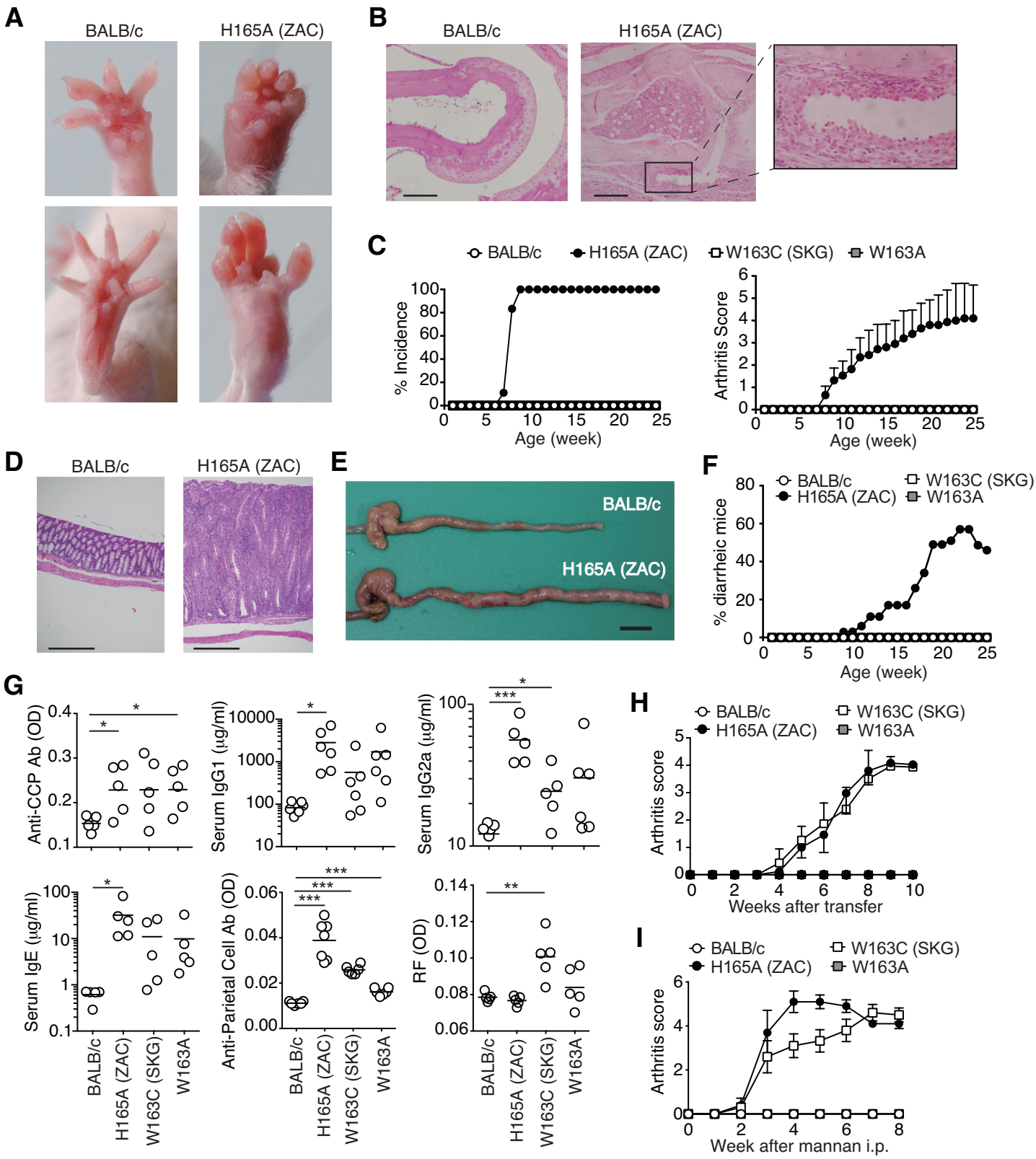
A
BALB/c
H165A (ZAC)
B
BALB/c
H165A (ZAC)
C
BALB/c
H165A (ZAC)
W163C (SKG)
W163A
% Incidence
Age (week)
Arthritis Score
Age (week)
D
BALB/c
H165A (ZAC)
E
BALB/c
H165A (ZAC)
F
BALB/c
H165A (ZAC)
W163C (SKG)
W163A
% diarrheic mice
Age (week)
G
Anti-CCP Ab (OD)
Serum IgG1 (μg/ml)
Serum IgG2a (μg/ml)
Serum IgE (μg/ml)
Anti-Parietal Cell Ab (OD)
RF (OD)
BALB/c
H165A (ZAC)
W163C (SKG)
W163A
H
BALB/c
H165A (ZAC)
W163C (SKG)
W163A
Arthritis score
Weeks after transfer
I
BALB/c
H165A (ZAC)
W163C (SKG)
W163A
Arthritis score
Week after mannan i.p.

Figure 2

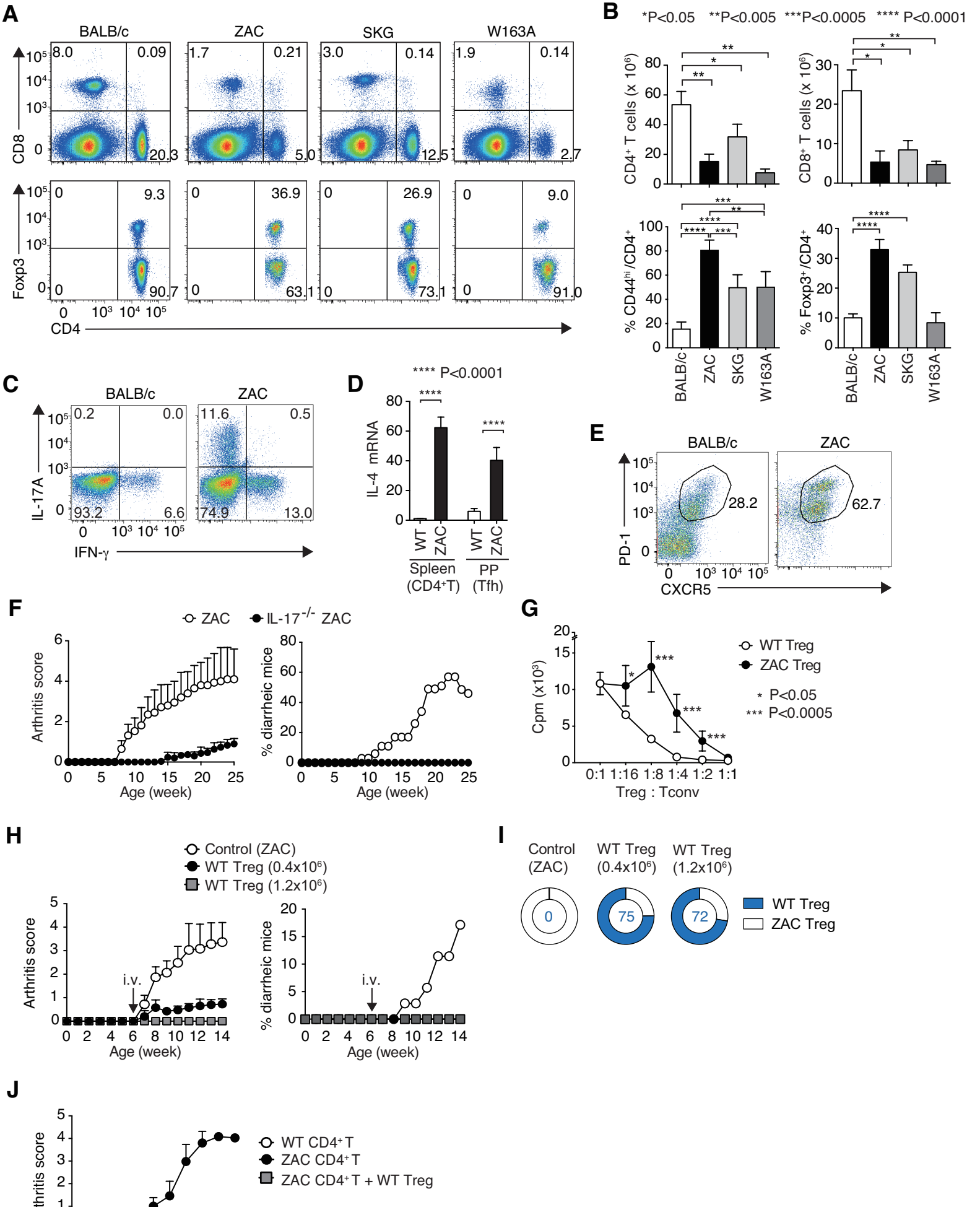
A
BALB/c
ZAC
SKG
W163A
CD8
Foxp3
CD4
B
*P<0.05 **P<0.005 ***P<0.0005 **** P<0.0001
CD4+ T cells (x 10^6)
CD8+ T cells (x 10^6)
% CD44hi/CD4+
% Foxp3+/CD4+
C
IL-17A
IFN-γ
D
**** P<0.0001
IL-4 mRNA
Spleen (CD4+T)
PP (Tfh)
E
PD-1
CXCR5
F
ZAC
IL-17-/- ZAC
Arthritis score
% diarrheic mice
Age (week)
G
WT Treg
ZAC Treg
* P<0.05
*** P<0.0005
Cpm (x10^3)
Treg : Tconv
H
Control (ZAC)
WT Treg (0.4x10^6)
WT Treg (1.2x10^6)
i.v.
I
Control (ZAC)
WT Treg (0.4x10^6)
WT Treg (1.2x10^6)
WT Treg
ZAC Treg
J
WT CD4+T
ZAC CD4+T
ZAC CD4+T + WT Treg
Weeks after transfer

Figure 3

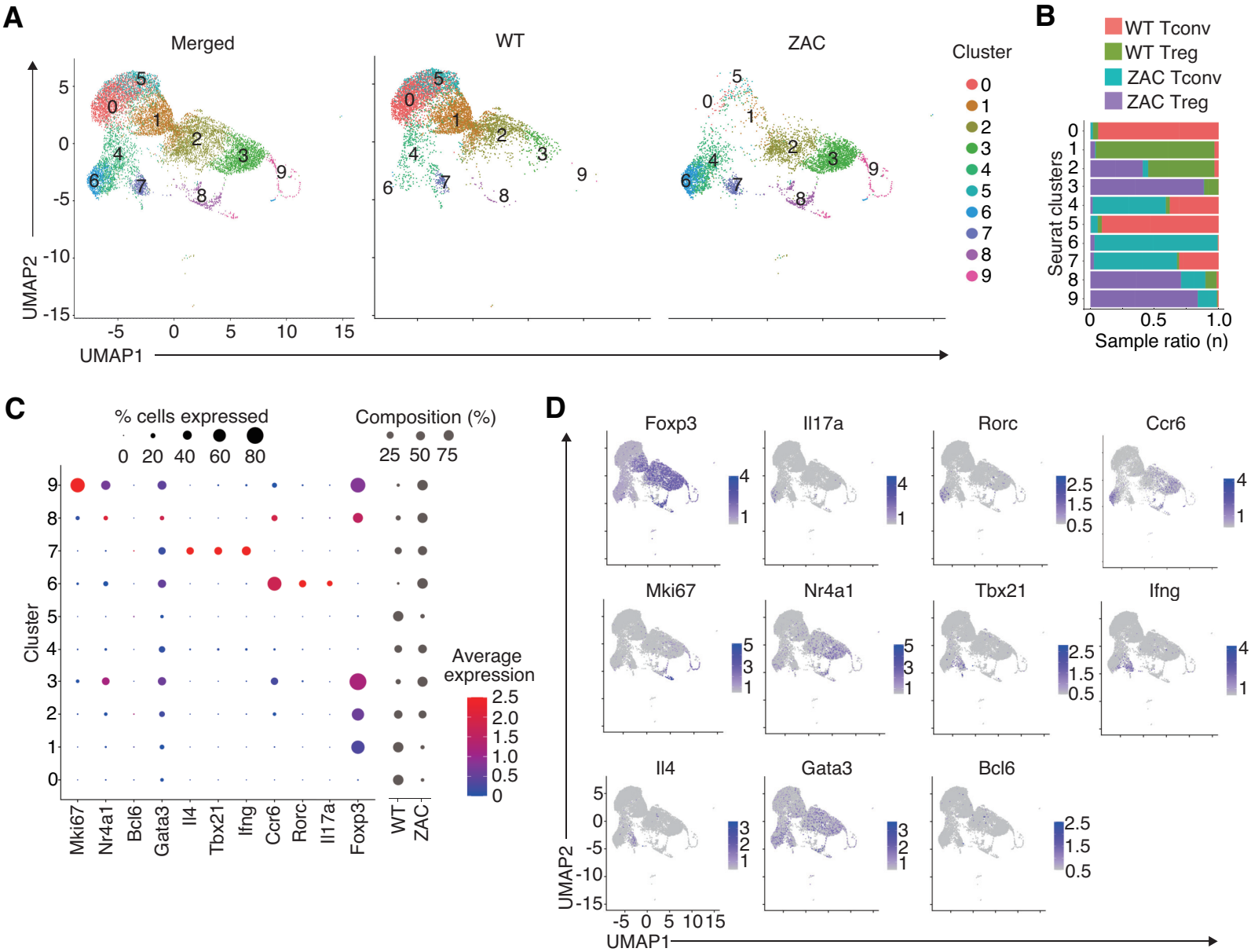
A
Merged
WT
ZAC
Cluster
UMAP2
UMAP1
B
WT Tconv
WT Treg
ZAC Tconv
ZAC Treg
Seurat clusters
Sample ratio (n)
C
% cells expressed
Composition (%)
Average expression
Cluster
Mki67
Nr4a1
Bcl6
Gata3
Il4
Tbx21
Ifng
Ccr6
Rorc
Il17a
Foxp3
WT
ZAC
D
Foxp3
Il17a
Rorc
Ccr6
Mki67
Nr4a1
Tbx21
Ifng
Il4
Gata3
Bcl6
UMAP2
UMAP1

Figure 4

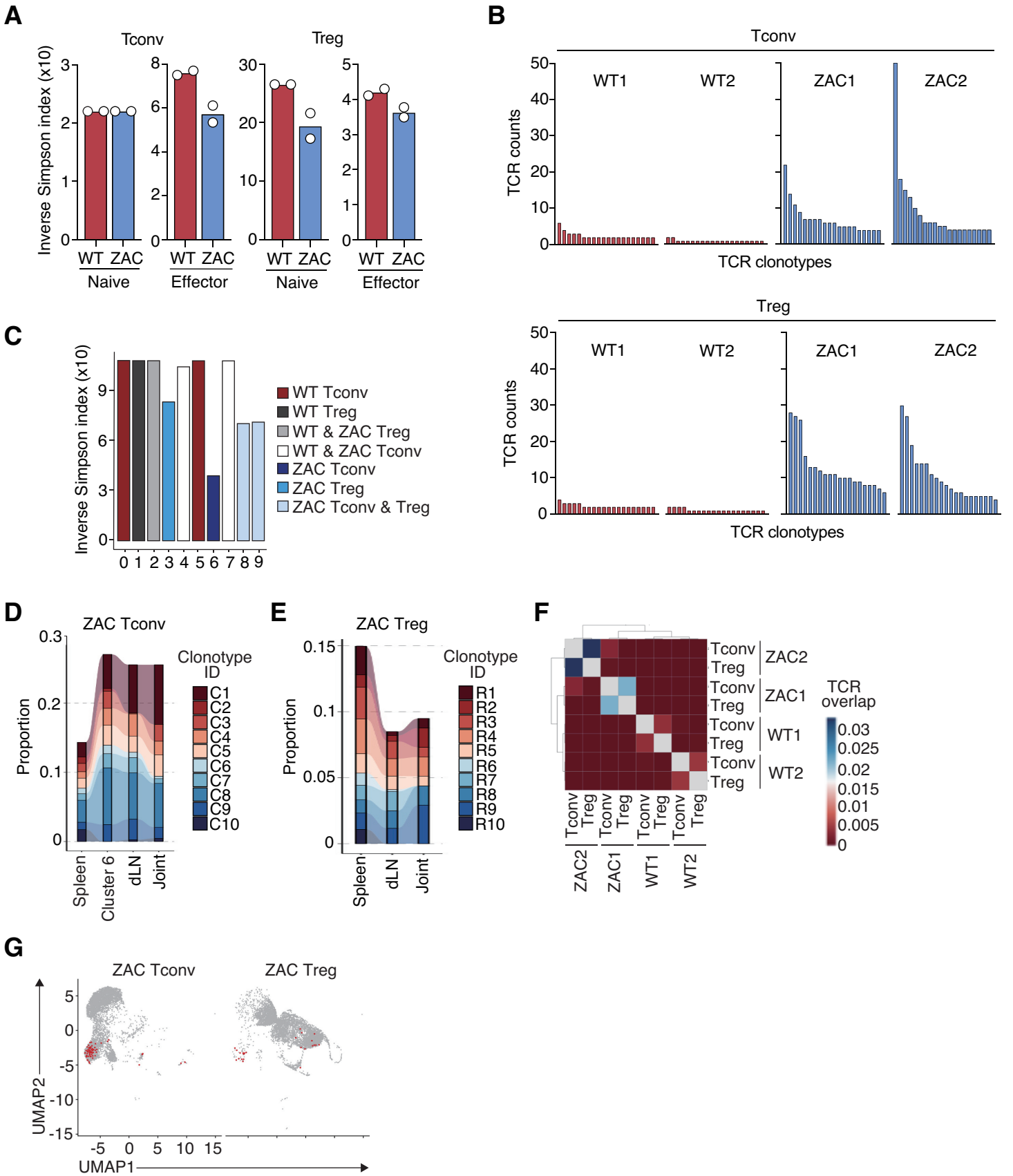
A
Tconv
Treg
Inverse Simpson index (x10)
WT ZAC
Naive
Effector
B
Tconv
WT1
WT2
ZAC1
ZAC2
TCR counts
TCR clonotypes
Treg
C
Inverse Simpson index (x10)
WT Tconv
WT Treg
WT & ZAC Treg
WT & ZAC Tconv
ZAC Tconv
ZAC Treg
ZAC Tconv & Treg
D
ZAC Tconv
Proportion
Clonotype ID
Spleen
Cluster 6
dLN
Joint
E
ZAC Treg
F
Tconv
Treg
TCR overlap
G
ZAC Tconv
ZAC Treg
UMAP2
UMAP1

Figure 5

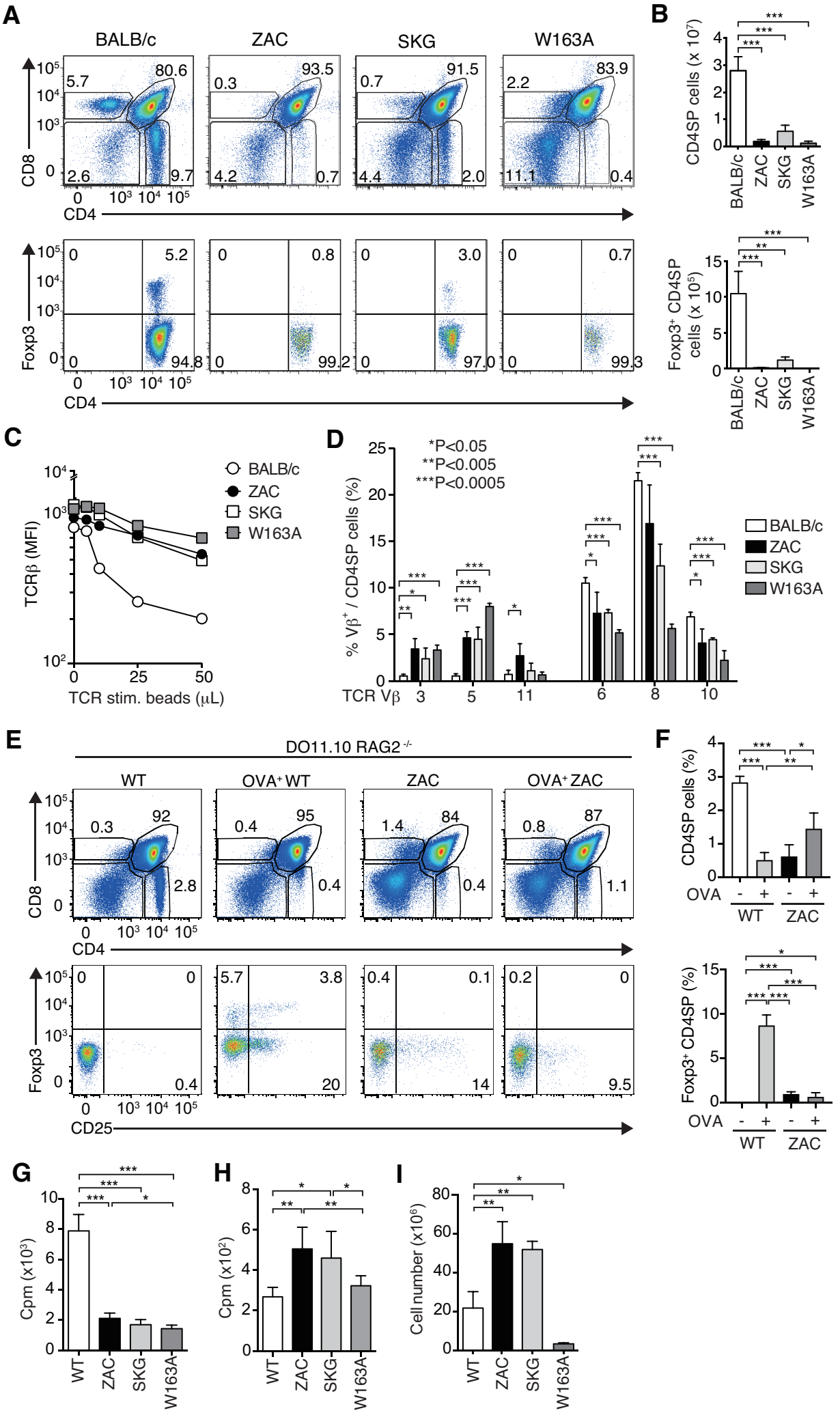
A
BALB/c
ZAC
SKG
W163A
CD8
CD4
Foxp3
5.7
80.6
2.6
9.7
0.3
93.5
4.2
0.7
0.7
91.5
4.4
2.0
2.2
83.9
11.1
0.4
5.2
94.8
0.8
99.2
3.0
97.0
0.7
99.3
B
CD4SP cells (x 10⁷)
Foxp3⁺ CD4SP cells (x 10⁵)
C
TCRβ (MFI)
TCR stim. beads (μL)
D
*P<0.05
**P<0.005
***P<0.0005
% Vβ⁺ / CD4SP cells (%)
TCR Vβ
3
5
11
6
8
10
E
DO11.10 RAG2 -/-
WT
OVA⁺ WT
ZAC
OVA⁺ ZAC
0.3
92
2.8
0.4
95
0.4
1.4
84
0.4
0.8
87
1.1
0.4
5.7
3.8
20
0.4
14
0.2
9.5
CD25
F
CD4SP cells (%)
Foxp3⁺ CD4SP (%)
OVA
WT
ZAC
G
Cpm (x10³)
H
Cpm (x10²)
I
Cell number (x10⁶)

Figure 6

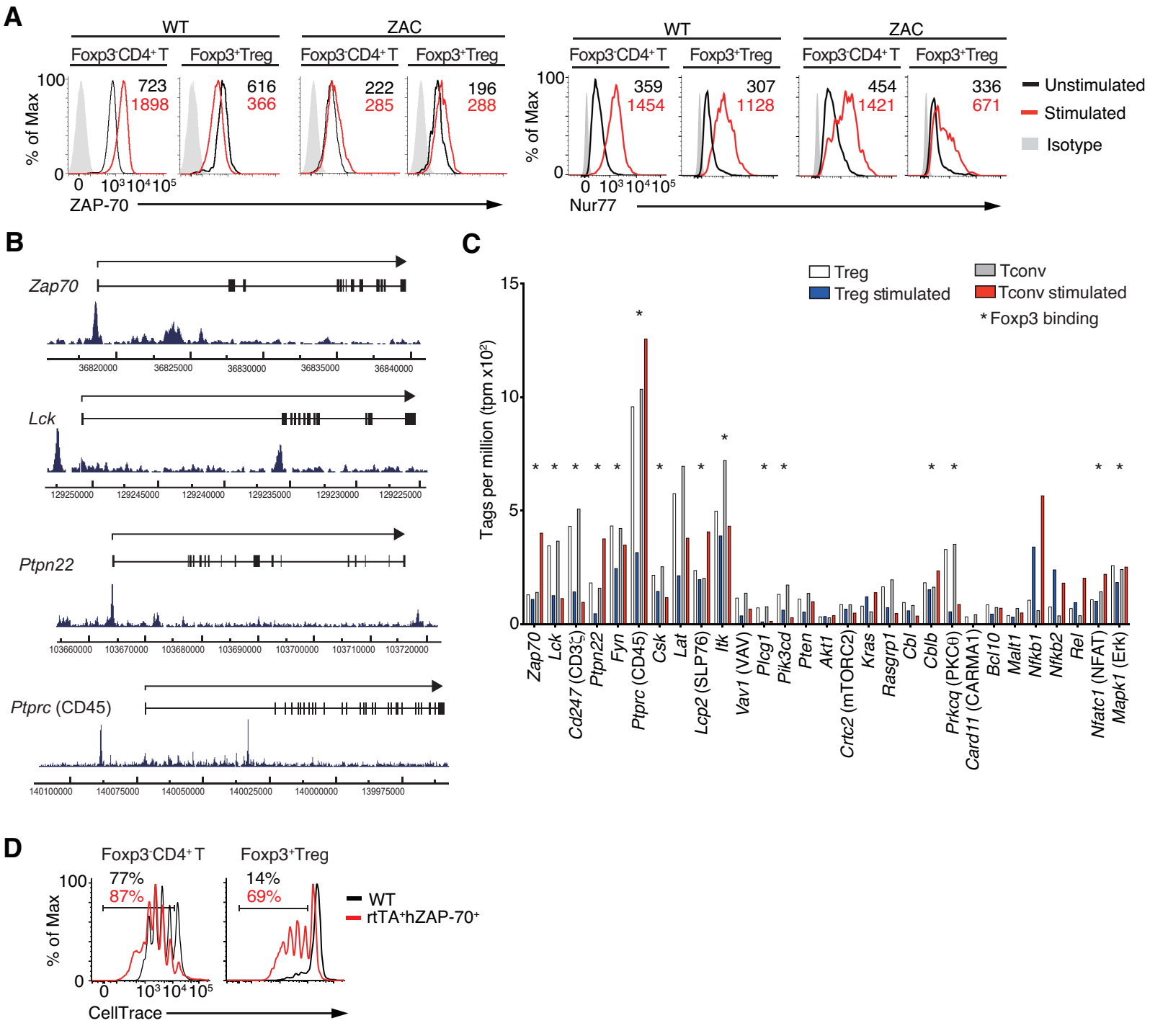
A
WT
ZAC
Foxp3-CD4+ T
Foxp3+Treg
% of Max
ZAP-70
Nur77
723
1898
616
366
222
285
196
288
359
1454
307
1128
454
1421
336
671
Unstimulated
Stimulated
Isotype
B
Zap70
Lck
Ptpn22
Ptprc (CD45)
C
Treg
Treg stimulated
Tconv
Tconv stimulated
* Foxp3 binding
Tags per million (tpm x10²)
Zap70
Lck
Cd247 (CD3ζ)
Ptpn22
Fyn
Ptprc (CD45)
Csk
Lat
Lcp2 (SLP76)
Itk
Vav1 (VAV)
Plcg1
Pik3cd
Pten
Akt1
Crtc2 (mTORC2)
Kras
Rasgrp1
Cbl
Cblb
Prkcq (PKCθ)
Card11 (CARMA1)
Bcl10
Malt1
Nfkb1
Nfkb2
Rel
Nfatc1 (NFAT)
Mapk1 (Erk)
D
Foxp3-CD4+ T
Foxp3+Treg
77%
87%
14%
69%
WT
rtTA+hZAP-70+
CellTrace

Figure 7

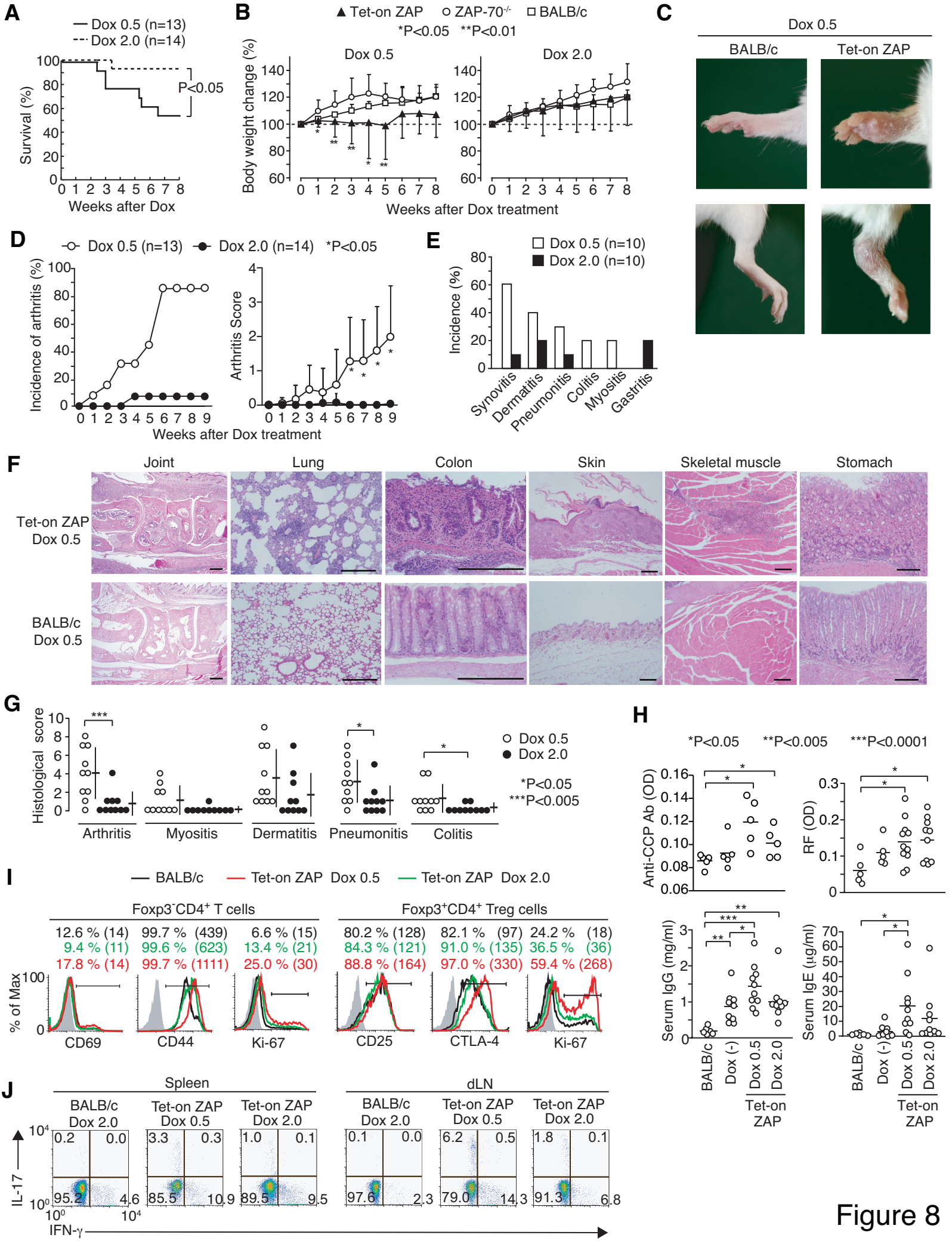
A
Dox 0.5 (n=13)
Dox 2.0 (n=14)
Survival (%)
P<0.05
Weeks after Dox
B
Tet-on ZAP
ZAP-70-/-
BALB/c
*P<0.05 **P<0.01
Dox 0.5
Dox 2.0
Body weight change (%)
Weeks after Dox treatment
C
Dox 0.5
BALB/c
Tet-on ZAP
D
Dox 0.5 (n=13)
Dox 2.0 (n=14)
*P<0.05
Incidence of arthritis (%)
Arthritis Score
Weeks after Dox treatment
E
Dox 0.5 (n=10)
Dox 2.0 (n=10)
Incidence (%)
Synovitis
Dermatitis
Pneumonitis
Colitis
Myositis
Gastritis
F
Joint
Lung
Colon
Skin
Skeletal muscle
Stomach
Tet-on ZAP Dox 0.5
BALB/c Dox 0.5
G
Histological score
Arthritis
Myositis
Dermatitis
Pneumonitis
Colitis
Dox 0.5
Dox 2.0
*P<0.05
***P<0.005
H
*P<0.05 **P<0.005 ***P<0.0001
Anti-CCP Ab (OD)
RF (OD)
Serum IgG (mg/ml)
Serum IgE (μg/ml)
BALB/c
Dox (-)
Dox 0.5
Dox 2.0
Tet-on ZAP
I
BALB/c
Tet-on ZAP Dox 0.5
Tet-on ZAP Dox 2.0
Foxp3-CD4+ T cells
Foxp3+CD4+ Treg cells
12.6 % (14) 99.7 % (439) 6.6 % (15)
9.4 % (11) 99.6 % (623) 13.4 % (21)
17.8 % (14) 99.7 % (1111) 25.0 % (30)
80.2 % (128) 82.1 % (97) 24.2 % (18)
84.3 % (121) 91.0 % (135) 36.5 % (36)
88.8 % (164) 97.0 % (330) 59.4 % (268)
% of Max
CD69
CD44
Ki-67
CD25
CTLA-4
Ki-67
J
Spleen
dLN
BALB/c Dox 2.0
Tet-on ZAP Dox 0.5
Tet-on ZAP Dox 2.0
0.2 0.0 95.2 4.6
3.3 0.3 85.5 10.9
1.0 0.1 89.5 9.5
0.1 0.0 97.6 2.3
6.2 0.5 79.0 14.3
1.8 0.1 91.3 6.8
IL-17
IFN-γ

Figure 8

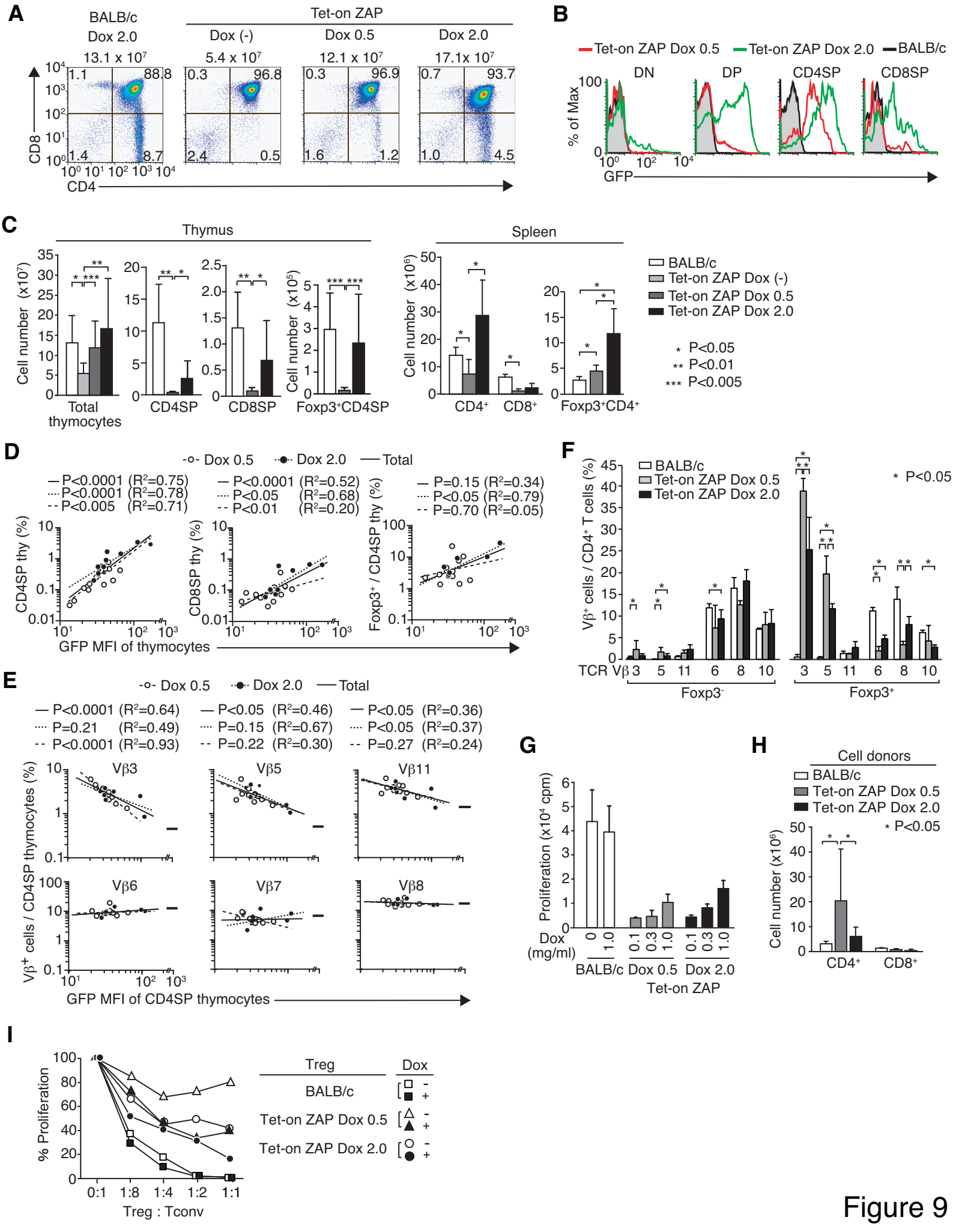
A
BALB/c
Dox 2.0
13.1 x 10^7
Tet-on ZAP
Dox (-)
5.4 x 10^7
Dox 0.5
12.1 x 10^7
Dox 2.0
17.1x 10^7
1.1
88.8
1.4
8.7
0.3
96.8
2.4
0.5
0.3
96.9
1.6
1.2
0.7
93.7
1.0
4.5
CD8
CD4
B
Tet-on ZAP Dox 0.5
Tet-on ZAP Dox 2.0
BALB/c
DN
DP
CD4SP
CD8SP
% of Max
GFP
C
Thymus
Spleen
Cell number (x10^7)
Cell number (x10^5)
Cell number (x10^6)
Total thymocytes
CD4SP
CD8SP
Foxp3+CD4SP
CD4+
CD8+
Foxp3+CD4+
BALB/c
Tet-on ZAP Dox (-)
Tet-on ZAP Dox 0.5
Tet-on ZAP Dox 2.0
* P<0.05
** P<0.01
*** P<0.005
D
Dox 0.5
Dox 2.0
Total
P<0.0001 (R²=0.75)
P<0.0001 (R²=0.78)
P<0.005 (R²=0.71)
P<0.0001 (R²=0.52)
P<0.05 (R²=0.68)
P<0.01 (R²=0.20)
P=0.15 (R²=0.34)
P<0.05 (R²=0.79)
P=0.70 (R²=0.05)
CD4SP thy (%)
CD8SP thy (%)
Foxp3+ / CD4SP thy (%)
GFP MFI of thymocytes
E
Dox 0.5
Dox 2.0
Total
P<0.0001 (R²=0.64)
P=0.21 (R²=0.49)
P<0.0001 (R²=0.93)
P<0.05 (R²=0.46)
P=0.15 (R²=0.67)
P=0.22 (R²=0.30)
P<0.05 (R²=0.36)
P<0.05 (R²=0.37)
P=0.27 (R²=0.24)
Vβ3
Vβ5
Vβ11
Vβ6
Vβ7
Vβ8
Vβ+ cells / CD4SP thymocytes (%)
GFP MFI of CD4SP thymocytes
F
BALB/c
Tet-on ZAP Dox 0.5
Tet-on ZAP Dox 2.0
* P<0.05
Vβ+ cells / CD4+ T cells (%)
TCR Vβ 3 5 11 6 8 10
Foxp3-
Foxp3+
G
Proliferation (x10^4 cpm)
Dox (mg/ml)
0 1.0 0.1 0.3 1.0 0.1 0.3 1.0
BALB/c Dox 0.5 Dox 2.0
Tet-on ZAP
H
Cell donors
BALB/c
Tet-on ZAP Dox 0.5
Tet-on ZAP Dox 2.0
* P<0.05
Cell number (x10^6)
CD4+
CD8+
I
% Proliferation
Treg : Tconv
0:1 1:8 1:4 1:2 1:1
Treg
Dox
BALB/c
Tet-on ZAP Dox 0.5
Tet-on ZAP Dox 2.0

Figure 9

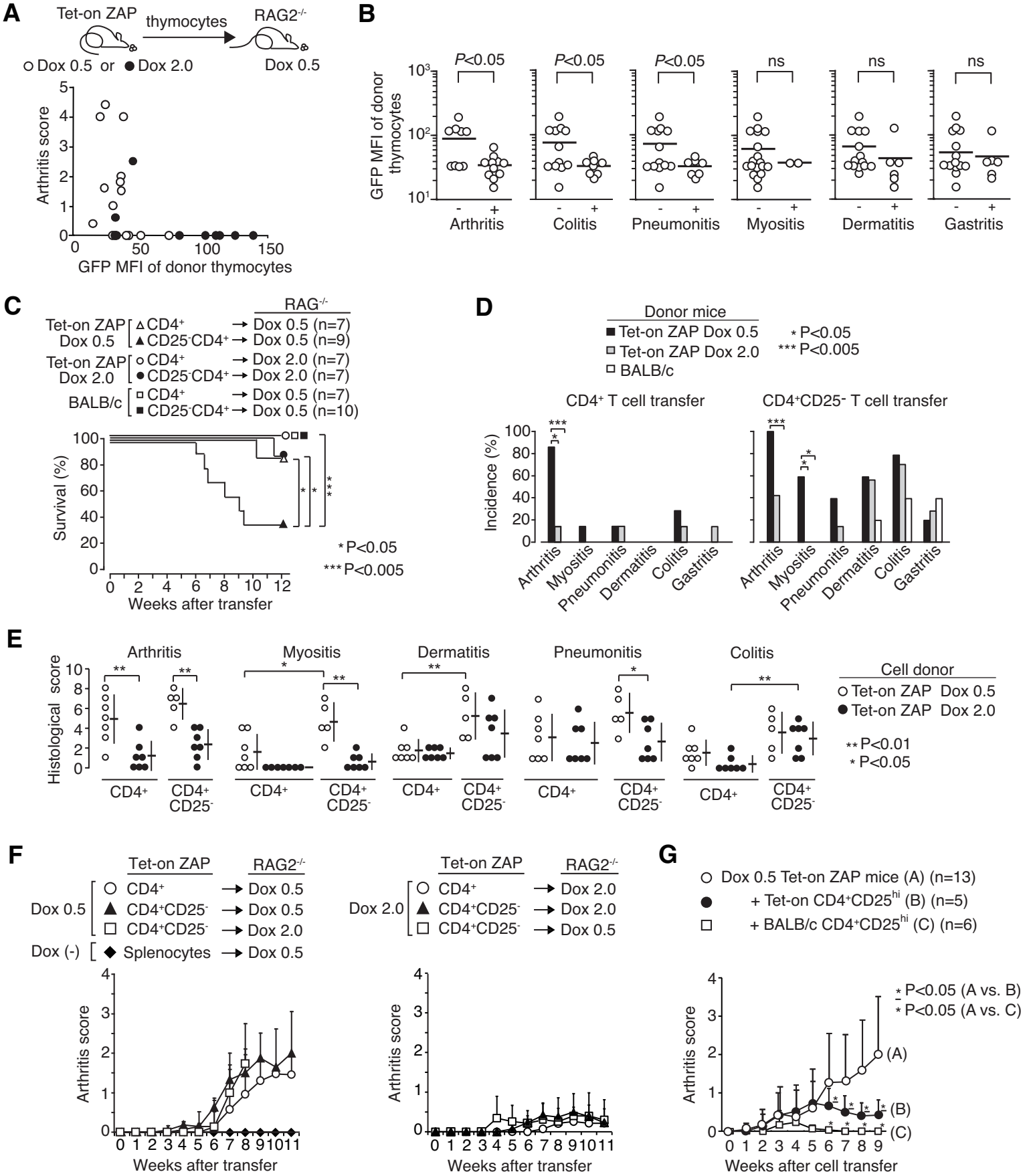
A
Tet-on ZAP
thymocytes
RAG2-/-
Dox 0.5 or Dox 2.0
Dox 0.5
Arthritis score
GFP MFI of donor thymocytes
B
GFP MFI of donor thymocytes
P<0.05
P<0.05
P<0.05
ns
ns
ns
Arthritis
Colitis
Pneumonitis
Myositis
Dermatitis
Gastritis
C
RAG-/-
Tet-on ZAP Dox 0.5
CD4+ → Dox 0.5 (n=7)
CD25-CD4+ → Dox 0.5 (n=9)
Tet-on ZAP Dox 2.0
CD4+ → Dox 2.0 (n=7)
CD25-CD4+ → Dox 2.0 (n=7)
BALB/c
CD4+ → Dox 0.5 (n=7)
CD25-CD4+ → Dox 0.5 (n=10)
Survival (%)
Weeks after transfer
* P<0.05
*** P<0.005
D
Donor mice
Tet-on ZAP Dox 0.5
Tet-on ZAP Dox 2.0
BALB/c
* P<0.05
*** P<0.005
CD4+ T cell transfer
CD4+CD25- T cell transfer
Incidence (%)
Arthritis
Myositis
Pneumonitis
Dermatitis
Colitis
Gastritis
E
Histological score
Arthritis
Myositis
Dermatitis
Pneumonitis
Colitis
CD4+
CD4+ CD25-
Cell donor
Tet-on ZAP Dox 0.5
Tet-on ZAP Dox 2.0
** P<0.01
* P<0.05
F
Tet-on ZAP
RAG2-/-
Dox 0.5
CD4+ → Dox 0.5
CD4+CD25- → Dox 0.5
CD4+CD25- → Dox 2.0
Dox (-)
Splenocytes → Dox 0.5
Dox 2.0
CD4+ → Dox 2.0
CD4+CD25- → Dox 2.0
CD4+CD25- → Dox 0.5
Arthritis score
Weeks after transfer
G
Dox 0.5 Tet-on ZAP mice (A) (n=13)
+ Tet-on CD4+CD25hi (B) (n=5)
+ BALB/c CD4+CD25hi (C) (n=6)
* P<0.05 (A vs. B)
* P<0.05 (A vs. C)
(A)
(B)
(C)
Arthritis score
Weeks after cell transfer

Figure 10

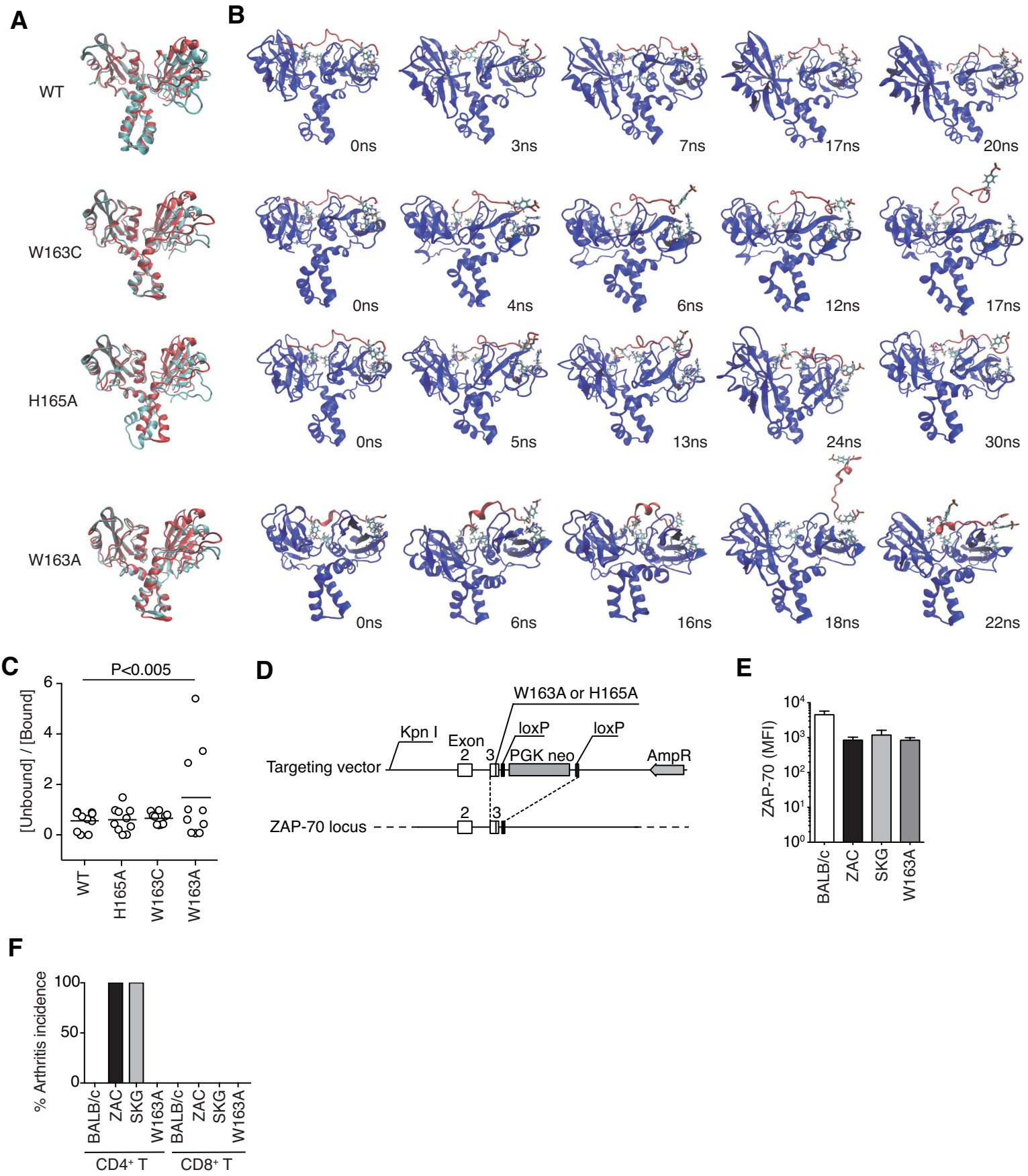

Supplemental Figure S1

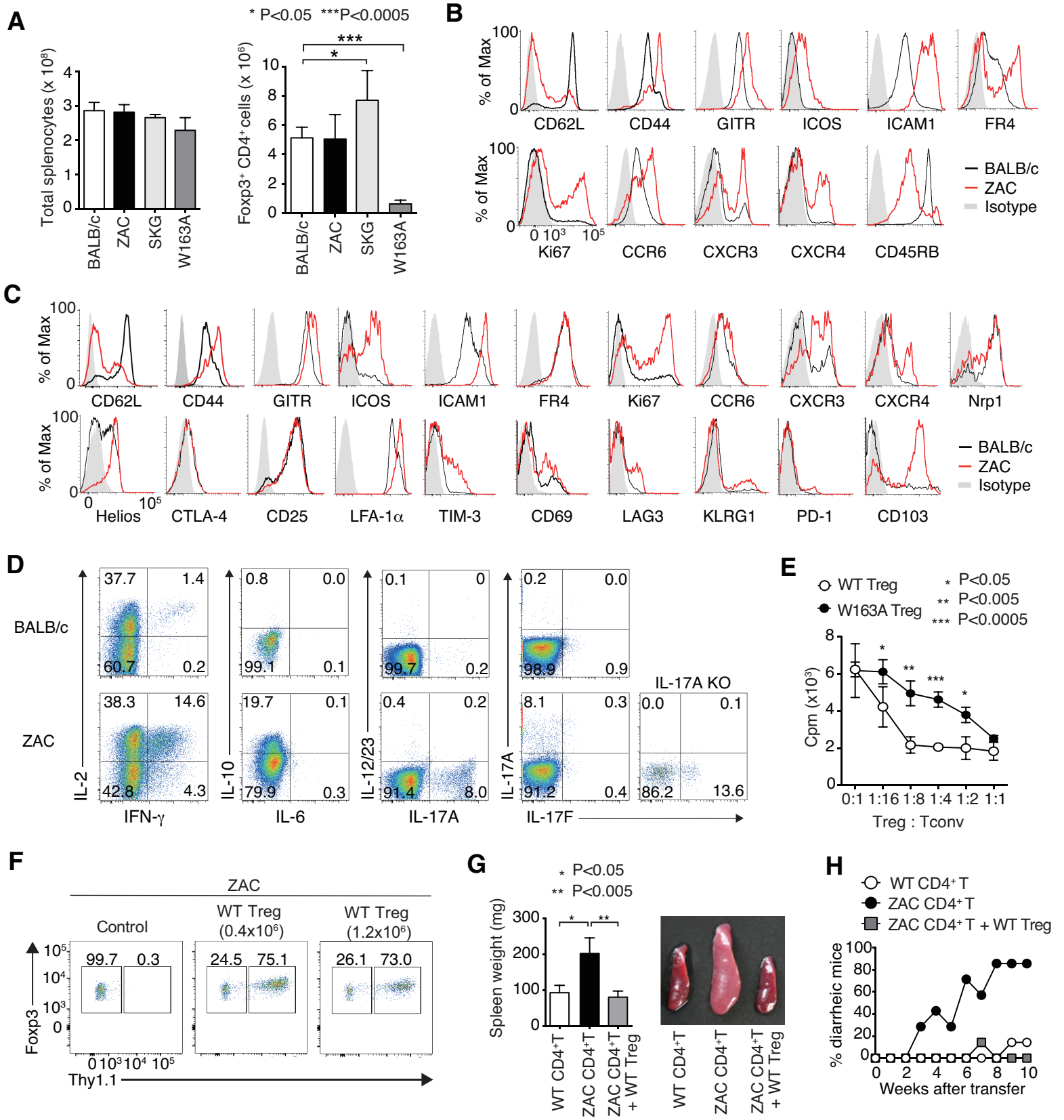

Supplemental Figure S2

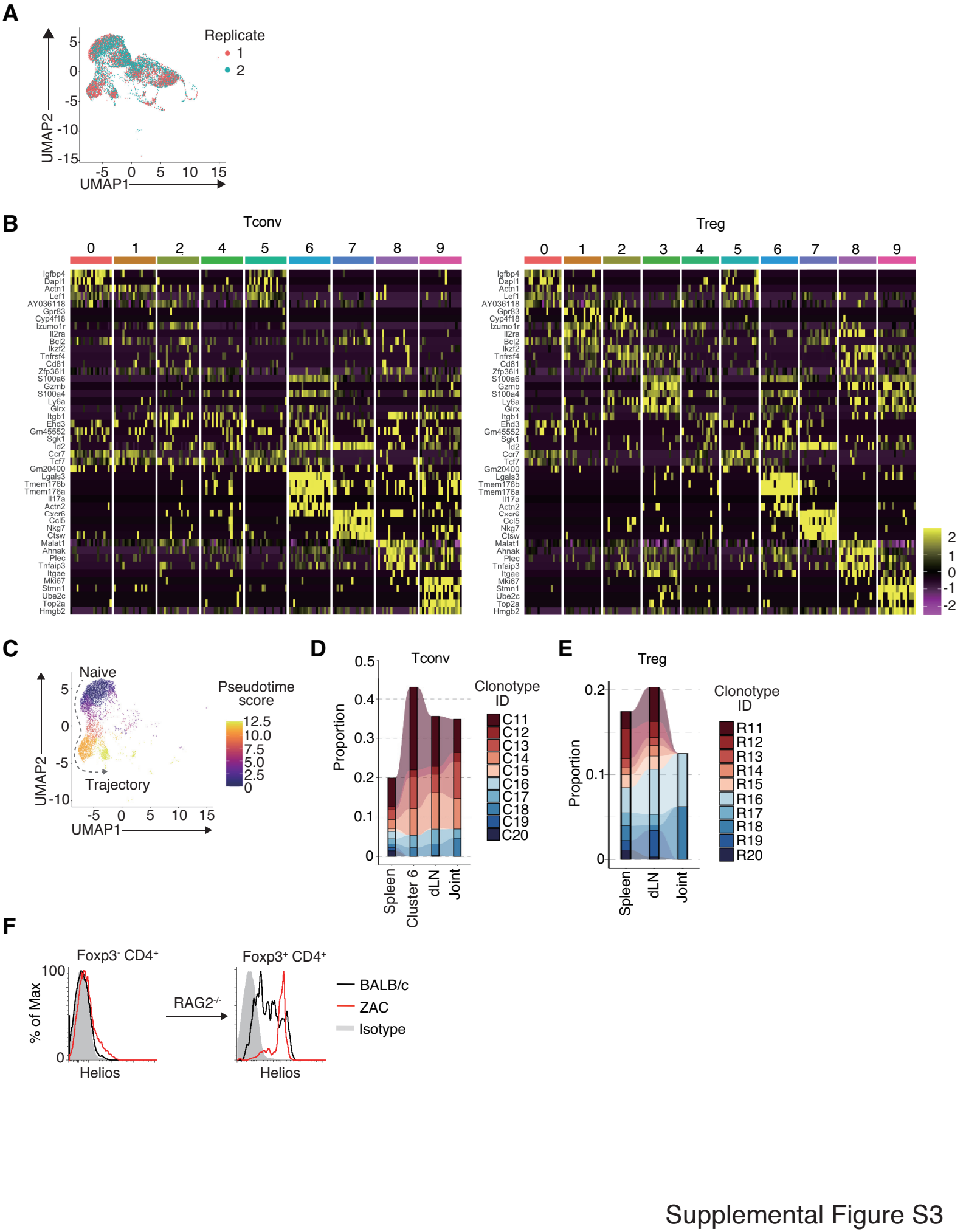

Supplemental Figure S3

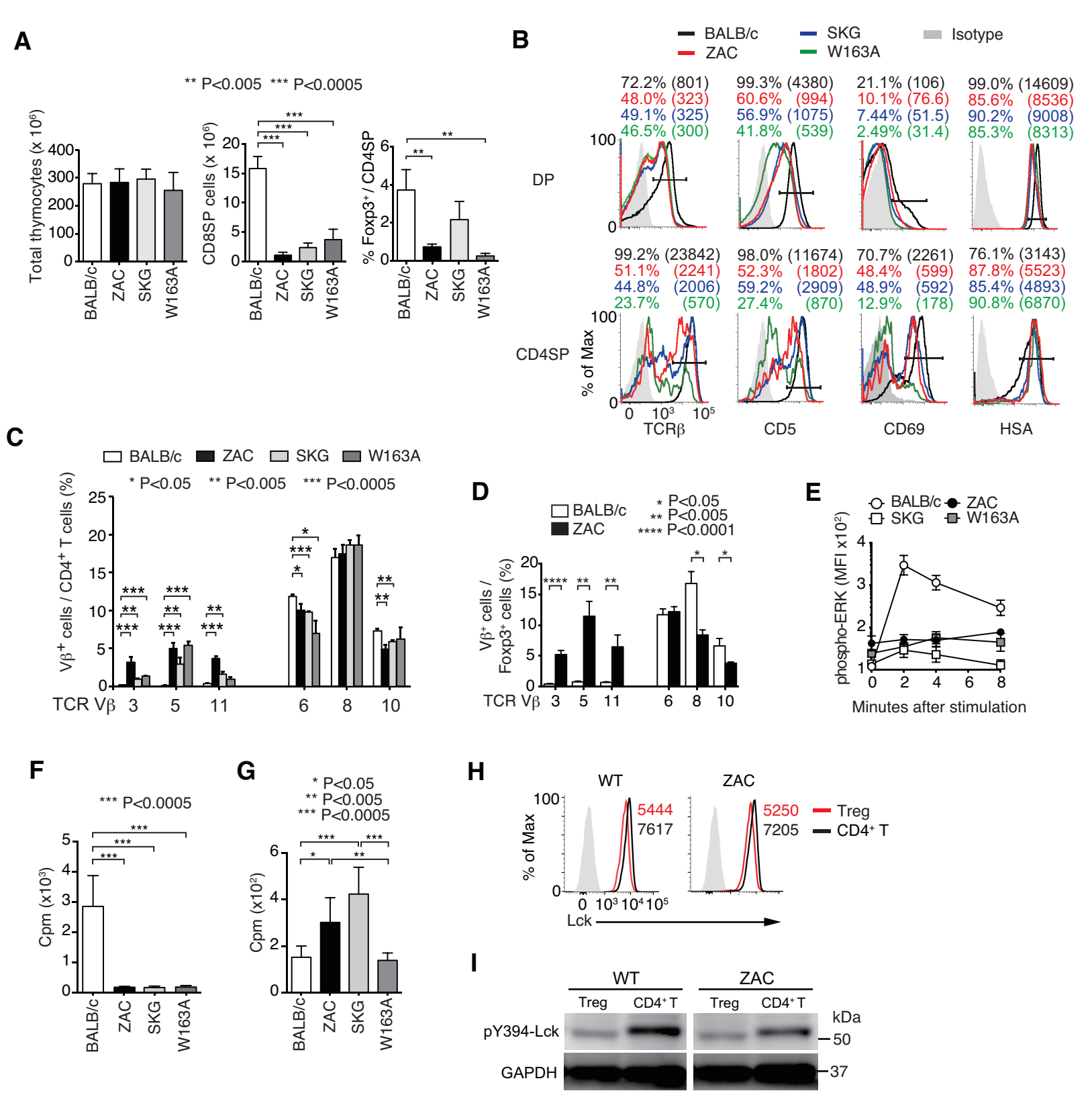

Supplemental Figure S4

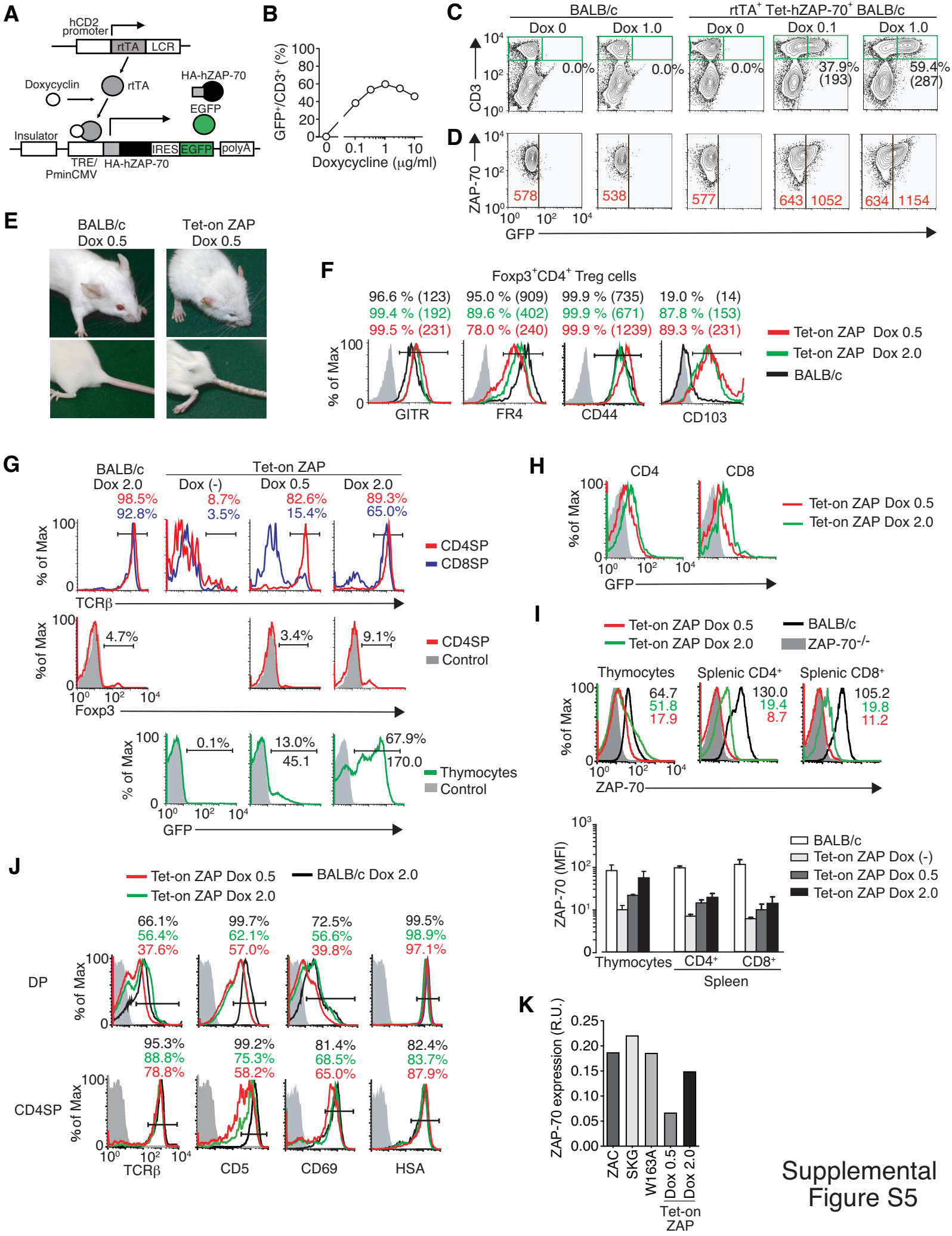
A
hCD2 promoter
rtTA
LCR
Doxycyclin
rtTA
HA-hZAP-70
EGFP
Insulator
IRES
EGFP
polyA
TRE/ PminCMV
HA-hZAP-70
B
GFP+/CD3+ (%)
Doxycycline (μg/ml)
C
BALB/c
rtTA+ Tet-hZAP-70+ BALB/c
Dox 0
Dox 1.0
Dox 0.1
CD3
0.0%
37.9% (193)
59.4% (287)
D
ZAP-70
GFP
578
538
577
643
1052
634
1154
E
BALB/c Dox 0.5
Tet-on ZAP Dox 0.5
F
Foxp3+CD4+ Treg cells
96.6 % (123)
99.4 % (192)
99.5 % (231)
95.0 % (909)
89.6 % (402)
78.0 % (240)
99.9 % (735)
99.9 % (671)
99.9 % (1239)
19.0 % (14)
87.8 % (153)
89.3 % (231)
% of Max
GITR
FR4
CD44
CD103
Tet-on ZAP Dox 0.5
Tet-on ZAP Dox 2.0
BALB/c
G
BALB/c Dox 2.0
Tet-on ZAP
Dox (-)
Dox 0.5
Dox 2.0
98.5%
92.8%
8.7%
3.5%
82.6%
15.4%
89.3%
65.0%
TCRβ
CD4SP
CD8SP
4.7%
3.4%
9.1%
Foxp3
Control
0.1%
13.0%
45.1
67.9%
170.0
Thymocytes
GFP
H
CD4
CD8
GFP
I
Tet-on ZAP Dox 0.5
Tet-on ZAP Dox 2.0
BALB/c
ZAP-70-/-
Thymocytes
Splenic CD4+
Splenic CD8+
64.7
51.8
17.9
130.0
19.4
8.7
105.2
19.8
11.2
ZAP-70
ZAP-70 (MFI)
BALB/c
Tet-on ZAP Dox (-)
Tet-on ZAP Dox 0.5
Tet-on ZAP Dox 2.0
Thymocytes
CD4+
CD8+
Spleen
J
Tet-on ZAP Dox 0.5
Tet-on ZAP Dox 2.0
BALB/c Dox 2.0
DP
CD4SP
66.1%
56.4%
37.6%
99.7%
62.1%
57.0%
72.5%
56.6%
39.8%
99.5%
98.9%
97.1%
95.3%
88.8%
78.8%
99.2%
75.3%
58.2%
81.4%
68.5%
65.0%
82.4%
83.7%
87.9%
TCRβ
CD5
CD69
HSA
K
ZAP-70 expression (R.U.)
ZAC
SKG
W163A
Dox 0.5
Dox 2.0
Tet-on ZAP
Supplemental Figure S5